

Article

Crystal Structure Prediction of the Novel Cr₂SiN₄ Compound via Global Optimization, Data Mining, and the PCAE Method

Tamara Škundrić^{1,2}, Dejan Zagorac^{1,2,*}, Johann Christian Schön³, Milan Pejić^{1,2} and Branko Matović^{1,2}

¹ Materials Science Laboratory, Institute of Nuclear Sciences “Vinča”, University of Belgrade, National Institute of the Republic of Serbia, 11351 Belgrade, Serbia; tamara.skundric@vinca.rs (T.Š.); milan.pejic@yahoo.com (M.P.); mato@vinca.rs (B.M.)

² Center for the Synthesis, Processing and Characterization of Materials for Use in Extreme Conditions “CextremeLab”, 11001 Belgrade, Serbia

³ Max Planck Institute for Solid State Research, Heisenbergstr. 1, D-70569 Stuttgart, Germany; C.Schoen@fkf.mpg.de

* Correspondence: dzagorac@vin.bg.ac.rs

Abstract: A number of studies have indicated that the implementation of Si in CrN can significantly improve its performance as a protective coating. As has been shown, the Cr-Si-N coating is comprised of two phases, where nanocrystalline CrN is embedded in a Si₃N₄ amorphous matrix. However, these earlier experimental studies reported only Cr-Si-N in thin films. Here, we present the first investigation of possible bulk Cr-Si-N phases of composition Cr₂SiN₄. To identify the possible modifications, we performed global explorations of the energy landscape combined with data mining and the Primitive Cell approach for Atom Exchange (PCAE) method. After ab initio structural refinement, several promising low energy structure candidates were confirmed on both the GGA-PBE and the LDA-PZ levels of calculation. Global optimization yielded six energetically favorable structures and five modifications possible to be observed in extreme conditions. Data mining based searches produced nine candidates selected as the most relevant ones, with one of them representing the global minimum in the Cr₂SiN₄. Additionally, employing the Primitive Cell approach for Atom Exchange (PCAE) method, we found three more promising candidates in this system, two of which are monoclinic structures, which is in good agreement with results from the closely related Si₃N₄ system, where some novel monoclinic phases have been predicted in the past.

Keywords: Cr-Si-N compounds; structure prediction; global optimization; computational studies



Citation: Škundrić, T.; Zagorac, D.; Schön, J.C.; Pejić, M.; Matović, B. Crystal Structure Prediction of the Novel Cr₂SiN₄ Compound via Global Optimization, Data Mining, and the PCAE Method. *Crystals* **2021**, *11*, 891. <https://doi.org/10.3390/cryst11080891>

Academic Editors: Jaka Fajar Patriansyah and Amir H. Mosavi

Received: 25 June 2021

Accepted: 26 July 2021

Published: 30 July 2021

Publisher's Note: MDPI stays neutral with regard to jurisdictional claims in published maps and institutional affiliations.



Copyright: © 2021 by the authors. Licensee MDPI, Basel, Switzerland. This article is an open access article distributed under the terms and conditions of the Creative Commons Attribution (CC BY) license (<https://creativecommons.org/licenses/by/4.0/>).

1. Introduction

Tools and equipment used in metal and wood machining frequently experience severe damage during their usage, which leads to the urgent need for protective coatings to extend the lifetime of the machinery [1,2]. This particularly applies to marine equipment, where certain parts have to operate in challenging marine environments. Additionally, past nuclear accidents have led to an increase in research regarding nuclear materials and the development of coatings that can be used under such extreme conditions.

Transition metal nitrides are widely used as hard coatings, and, among them, CrN is one with many desired properties—high hardness, toughness, and corrosion resistance, good oxidation resistance, good adhesion strength, and excellent wear resistance [3–10]. However, due to its high friction coefficient, it does not perform well in some extreme conditions [2]. Delamination is considered to be critical to the wear failure of CrN coatings in seawater where microcracks play an important role in the evolution of delamination. [11].

Even though CrN is a well-established and very stable coating in wide use, the addition of alloying elements, such as Si, has been actively investigated to further improve its properties as a hard coating material [5,6,12–18]. Compared to CrN thin films, Cr-Si-N coatings exhibit lower friction coefficients and wear rates due to their low surface roughness.

In general, their tribological and mechanical characteristics show significant improvement under different environments and conditions (dry, humid, or aqueous; dynamic or static; ambient or high temperature; etc.) compared to CrN [3,19–27]. Due to the finer crystal structure, the addition of Si can also lead to the elimination of large flake pits, which were previously found on the wear trace of CrN coatings [26]. This increase in silicon content also leads to a change in the crystal structure of the coating, and the particle shape changes from triangular to circular with a distribution that tends to be uniform, while the density of the coating increases [28].

Four kinds of Cr-Si-N coatings are known that are considered to be harder than the CrN coating [28]. Nanocomposite Cr-Si-N thin films (usually in the form of nanocolumns or nanoclusters of CrN embedded in an amorphous Si_3N_4 matrix) also have higher hardness and oxidation resistance compared with CrN thin films [5,6,15–18,29]—their hardness can be increased by up to ~ 9 GPa [2,3,30,31], while their oxidation resistance is significantly improved at temperatures well above the oxidation limit of ~ 600 – 700 °C of CrN [6,32,33].

Epitaxially grown Cr-Si-N thin films that appear to constitute solid solutions of Si in CrN exhibit even higher hardness than less homogeneous nanocomposite Cr-Si-N thin films—a maximum hardness value of 51 GPa was obtained for 10 mol% Si in Cr-Si-N [34]. The increased hardness of Cr-Si-N is obtained due to the formation of a fine nanocomposite structure and the refinement of CrN crystallites [18,24] as well as to the dissolution of Si in CrN [34]. The decrease of friction is attributed to the formation of SiO_2 or $\text{Si}(\text{OH})_2$ layers in a humid environment, which plays a role as a self-lubricant, and by a smoother surface due to the Cr-Si-N amorphous phase [18,27]. Improved oxidation resistance can be explained by the formation of amorphous silicon oxide, which retards the diffusion of O as well as of Cr, Si, and N [29].

As its Si content increases, the structure of the Cr-Si-N coating changes from a crystalline to an amorphous state [35,36], and while the corrosion resistance constantly improves and the friction coefficient decreases, wear-resistance and hardness also improve until a certain Si content limit is reached beyond which the coatings start to deteriorate [25,34,37]. The electronic properties of Cr-Si-N thin films also change significantly depending on their chemical composition. While *fcc*-CrN exhibits metallic-like behavior, an increase of N or Si content leads to a more non-metallic character of the material [37].

Furthermore, investigations of the friction and wear properties of CrSi based coatings led to the conclusion that Cr-Si-N coatings showed better properties in comparison to the CrSi coatings [38]. Increasing the silicon content in these coatings led to the best friction and wear performance, which, in the case of an ATF system in a water environment, can reduce the wear volume by three orders of magnitude [38]. In summary, the Cr-Si-N coatings exhibit superior tribological performance due to their excellent toughness, high hardness, preferable adhesion, and good corrosion resistance [2], which all lead to the possibility of wide applications.

Gaining deeper insight into the structure–property relationship of the Cr-Si-N coating on the atomic level would greatly support the optimization of such coatings. As a first step, we focus on the possible existence of crystalline phases in the Cr/Si/N system. Considering the large hardness of Si_3N_4 , we chose the analogous composition Cr_2SiN_4 , where we would expect similarly high hardness as for Si_3N_4 itself. Thus, in this study, we identify feasible structure candidates of the composition Cr_2SiN_4 , using global optimization techniques, data-mining, and the Primitive Cell approach for Atom Exchange (PCAE) method, followed by careful re-optimizations of the candidates on the ab initio level.

2. Materials and Methods

To perform structure prediction and gain insight into the structural stability of the possible phases existing in the Cr_2SiN_4 system, a combination of global optimization (GO), data mining (DM), and the PCAE method has been used [39,40]. First, we performed global optimizations on the energy landscape of Cr_2SiN_4 using simulated annealing [41], within the G42+ code [42]. A fast computable robust empirical two-body potential consisting of

Lennard-Jones and exponentially damped Coulomb terms was employed to perform the GO searches with a reasonable computational effort [43]. Next, we have performed DM-based searches of the ICSD database [44,45] in order to find possible structure candidates for the unknown Cr_2SiN_4 compound.

We used the well-known KDD (knowledge discovery in databases) process, which involves selection, preprocessing, transformation, and interpretation/evaluation (or post-processing), and has been successfully used in previous studies [46–48]. Finally, the Primitive Cell approach for Atom Exchange (PCAE) method was employed for generating alternative structure candidates in the Cr_2SiN_4 compound. The PCAE method is simple, fast, and computationally inexpensive compared to the supercell approach [40].

In the current study, the starting modifications were taken from the related Si_3N_4 chemical system by first transforming the crystallographic (conventional) cell to the primitive cell, while keeping the symmetry and multiplicity of the atom positions (for more information, c.f. ref [40]). In the next stage, we replaced the number of atoms needed to obtain a certain stoichiometry ($2 \times \text{Si}$ by $2 \times \text{Cr}$ atoms) on the symmetry-related Wyckoff positions. Subsequently, an ab initio full structure optimization without symmetry constraints was performed.

After the structure candidates have been identified using the GO, DM and PCAE methods, each structure candidate has been subjected to local optimization on the ab initio level. Density functional theory (DFT) calculations of the total energy, and local optimizations (including volume, cell parameters, and atomic positions), were performed using the CRYSTAL17 code [49,50] based on linear combinations of atomic orbitals (LCAO). For the local optimization runs, we employed analytical gradients [51,52], and equation of state (EOS) calculations using polynomial fitting [49,50].

Local optimizations were performed on the DFT level employing two different functionals: the Local Density Approximation (LDA) with the Perdew–Zunger (PZ) correlation functional [53] and the Generalized Gradient Approximation (GGA) with the Perdew–Burke–Ernzerhof (PBE) functional [54] for comparison. It is reasonable to choose at least two different ab initio methods, to gain better insight into the quantitative validity of the results since no compounds of the composition Cr_2SiN_4 are available for comparison with the experiment [55–57].

An all-electron basis set based on Gaussian-type orbitals was employed in the case of chromium (Cr_86-411d41G_catti_1995) [58,59], silicon (Si_86-311G**_pascale_2005) [60,61], and nitrogen (N_6-21G*_dovesi_1990) [62,63]. The symmetries of the analyzed structures were determined using the SFND [64] and RGS [65] algorithms, and duplicate structures were removed using the CMPZ algorithm [66]; these three algorithms were implemented in the KPLOT code [67]. The optimized structures of various modifications were visualized using the Vesta3 program [68].

3. Results and Discussion

3.1. Global and Local Optimization Using Empirical and Ab Initio Energy Functions

Global optimizations were performed on the energy landscapes using empirical potentials for various numbers of formula units per simulation cell and for slightly varying ionic radii, yielding a total of 5000 structure candidates. Most of these global searches resulted in low-symmetry structure candidates (triclinic and monoclinic symmetry). After detailed statistical, structural, and crystallographic analysis, the most promising ones were submitted for local optimization on ab initio level. With further local optimization on the ab initio level, we have obtained the 11 most-relevant structure candidates from global optimization (GO).

Table 1 presents the energetic ranking of these new Cr_2SiN_4 phases using the GGA-PBE functional, where the α - Cr_2SiN_4 -type is the lowest in calculated total energy, and the $nf5$ - Cr_2SiN_4 -type the highest one. Moreover, we grouped the resulting GO structures into energetically favorable ones, ranging from the α - to the λ' - Cr_2SiN_4 phase, and non-favorable Cr_2SiN_4 modifications marked $nf1$ to $nf5$, which might be observed under extreme

conditions. In addition, each favorable structure candidate has been subjected to a DFT-LDA optimization with similar results in the energetic ranking (Table A2.)

Table 1. The total energy (in Eh) and relative energy values (in kcal/mol) compared to the global minimum (spinel structure taken as the zero of energy) of Cr_2SiN_4 modifications found after global optimization on an empirical potential level and locally optimized using the GGA-PBE functional.

Modification	Total Energy (Eh)	Relative Energy (kcal/mol)
α - Cr_2SiN_4 -type	−5193.474	20.708
β - Cr_2SiN_4 -type	−5193.438	43.298
δ - Cr_2SiN_4 -type	−5193.419	55.221
ϵ - Cr_2SiN_4 -type	−5193.413	58.986
λ - Cr_2SiN_4 -type	−5193.407	62.750
λ' - Cr_2SiN_4 -type	−5193.404	64.634
<i>nf1</i> - Cr_2SiN_4 -type	−5193.398	68.399
<i>nf2</i> - Cr_2SiN_4 -type	−5193.388	74.674
<i>nf3</i> - Cr_2SiN_4 -type	−5193.385	76.556
<i>nf4</i> - Cr_2SiN_4 -type	−5193.364	89.734
<i>nf5</i> - Cr_2SiN_4 -type	−5193.364	89.734

3.1.1. Structural Analysis of the Most Promising Modifications Found after Global Optimization (GO)

The energetically most favorable modification after global optimization is denoted as α - Cr_2SiN_4 -type and appears in the orthorhombic space group *Pma2* (no. 28) with unit cell parameters of $a = 5.54$, $b = 7.91$, and $c = 2.81$ Å on the GGA-PBE level of calculation. The α - Cr_2SiN_4 phase is visualized in Figure 1a, while full structural data of all favorable candidates are presented in Table 2 for calculations with the PBE functional, and in Table A1 for those computed with the LDA functional, respectively.

In the α -modification, chromium is six-fold coordinated by nitrogen, forming two different CrN_6 octahedra (with atom–atom distances of $\text{Cr}(1) 2 \times 1.82$ Å–N, 1×1.89 Å–N, 1×1.97 Å–N, 2×2.13 Å–N, $\text{Cr}(2) 2 \times 1.91$ Å–N, 2×1.95 Å–N, and 2×2.04 Å–N), while silicon is four-fold coordinated by nitrogen (with atom–atom distances of 2×1.77 Å–N and 2×1.71 Å–N) forming a tetrahedron. Moreover, the octahedra are connected by edges, while the tetrahedra are corner connected to them; additionally, the tetrahedra fall into two groups with opposite orientations.

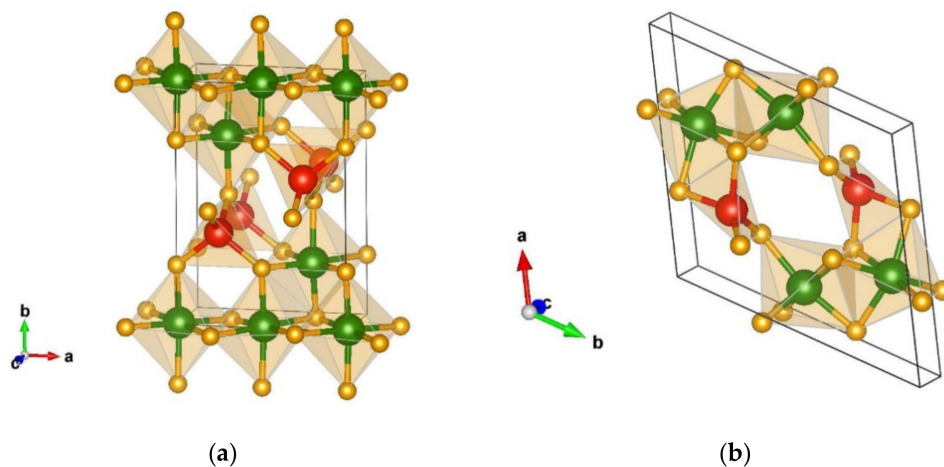


Figure 1. Visualization of favorable Cr_2SiN_4 modifications: (a) α - Cr_2SiN_4 -type in space group *Pma2* (no. 28); (b) β - Cr_2SiN_4 -type in space group *P-1* (no. 2). Green, red, and yellow spheres denote Cr, Si, and N atoms, respectively.

A second energetically favorable candidate obtained from GO is denoted as β - Cr_2SiN_4 -type. This triclinic structure appears in space group *P-1* (no. 2), with cell parameters

$a = 7.28$, $b = 7.79$, $c = 2.74$ Å, $\alpha = 93.66$, $\beta = 82.48$, and $\gamma = 120.64$ calculated with GGA-PBE, and is visualized in Figure 1b. In this structure, chromium has a six-fold coordination by nitrogen forming two different CrN_6 octahedra similar to the α -modification, while silicon is four-fold coordinated by nitrogen with interatomic distances for chromium (Cr(1) 2×1.88 Å-N, 1×1.93 Å-N, 1×1.99 Å-N, 1×2.00 Å-N, 1×2.12 Å-N, Cr(2) 1×1.86 Å-N, 1×1.90 Å-N, 1×1.94 Å-N, 1×1.96 Å-N, 1×2.02 Å-N, and 2×2.05 Å-N) and silicon (2×1.70 Å-N, 1×1.78 Å-N, and 1×1.81 Å-N).

As in the α - Cr_2SiN_4 -type modification, SiN_4 tetrahedra are oriented in different directions; however, in this modification, the CrN_6 octahedra are face-connected and lean against each other, thus, forming a void in the center of the structure that is reminiscent of zeolite formation.

Table 2. The modifications, space groups, unit cell parameters, and atomic positions for favorable Cr_2SiN_4 modifications found after global optimization and later locally optimized on the ab initio level using the GGA-PBE functional.

Modifications and Space Group	Cell Parameters	Position of Atoms
α - Cr_2SiN_4 -type <i>Pma2</i> No 28	$a = 5.54$ $b = 7.91$ $c = 2.81$	Cr 0.750000 0.245688 0.560883
		Cr 0.500000 0.000000 0.891696
		Si 0.750000 0.616760 0.000000
		N 0.750000 0.011076 0.423540
		N 0.750000 0.493745 0.499960
β - Cr_2SiN_4 -type <i>P-1</i> No 2	$a = 7.28$ $b = 7.79$ $c = 2.74$ $\alpha = 93.66$ $\beta = 82.48$ $\gamma = 120.64$	N 0.501383 0.244129 0.983362
		Cr 0.347419 0.861114 0.730714
		Cr 0.862711 0.520348 0.305878
		Si 0.627078 0.740684 0.913120
		N 0.050229 0.677562 0.759435
δ - Cr_2SiN_4 -type <i>P21/m</i> No 11	$a = 6.21$ $b = 3.82$ $c = 5.54$ $\beta = 116.24$	N 0.353428 0.666353 0.160724
		Cr 0.088537 0.750000 0.660564
		Cr 0.155145 0.750000 0.253988
		Si 0.613292 0.750000 0.917590
		N 0.639615 0.250000 0.413635
ϵ - Cr_2SiN_4 -type <i>P21/m</i> No 11	$a = 5.09$ $b = 2.89$ $c = 8.90$ $\beta = 90.20$	N 0.137168 0.250000 0.721296
		Cr 0.778189 0.250000 0.506779
		Cr 0.918790 0.750000 0.827219
		Si 0.419972 0.250000 0.798720
		N 0.567333 0.750000 0.861544
λ - Cr_2SiN_4 -type <i>Pm</i> No 6	$a = 5.07$ $b = 2.88$ $c = 9.27$ $\beta = 99.77$	N 0.897872 0.750000 0.121156
		Cr 0.060536 0.250000 0.368680
		Cr 0.951900 0.500000 0.415607
		Cr 0.698619 0.500000 0.708230
		Cr 0.291904 0.000000 0.722310
		Cr 0.507805 0.500000 0.040389
		Si 0.000000 0.000000 0.000000
		Si 0.455229 0.000000 0.394275
		N 0.535616 0.000000 0.585846
		N 0.455096 0.500000 0.844293
		N 0.704956 0.000000 0.076886
N 0.586474 0.500000 0.329108		
N 0.050793 0.500000 0.599924		
N 0.108035 0.000000 0.351718		
N 0.939400 0.000000 0.811337		
N 0.163111 0.500000 0.068461		

Table 2. Cont.

Modifications and Space Group	Cell Parameters	Position of Atoms
λ' -Cr ₂ SiN ₄ -type <i>Pm</i> No 6	a = 5.06 b = 2.87 c = 9.18 $\beta = 90.97$	Cr 0.166652 0.500000 0.355602
		Cr 0.889145 0.500000 0.685518
		Cr 0.307908 0.000000 0.681019
		Cr 0.485319 0.500000 0.980324
		Si 0.000000 0.000000 0.000000
		Si 0.670339 0.000000 0.395017
		N 0.676765 0.000000 0.583978
		N 0.498298 0.500000 0.794695
		N 0.665262 0.000000 0.039248
		N 0.812605 0.500000 0.324037
		N 0.176521 0.500000 0.552065
		N 0.351051 0.000000 0.317489
		N 0.015000 0.000000 0.810727
N 0.151227 0.500000 0.066773		

The next energetically favorable candidate found using global optimization is a monoclinic structure denoted as the δ -Cr₂SiN₄-type that crystallizes in space group *P21/m* (no. 11). This structure is presented in Figure 2a with unit cell parameters a = 6.21 b = 3.82 c = 5.54 Å, and $\beta = 116.24$, computed using the PBE functional (Table 2). Interestingly, in the δ -phase both, chromium and silicon are six-fold coordinated by nitrogen, with the octahedra being edge-connected, indicating that this candidate might be a high-pressure phase.

Additionally, the interatomic distances in the two different CrN₆ octahedra are Cr(1) 1 × 1.91 Å-N, 2 × 1.94 Å-N, 1 × 1.95 Å-N, 1 × 1.97 Å-N, 1 × 2.06 Å-N, Cr(2) 1 × 1.71 Å-N, 1 × 1.88 Å-N, 2 × 1.95 Å-N, 1 × 2.12 Å-N, and 1 × 2.27 Å-N, and the atom–atom distances in the SiN₆ octahedra are 1 × 1.81 Å-N, 1 × 1.93 Å-N, 2 × 1.92 Å-N, 1 × 1.85 Å-N, and 1 × 1.91 Å-N, respectively.

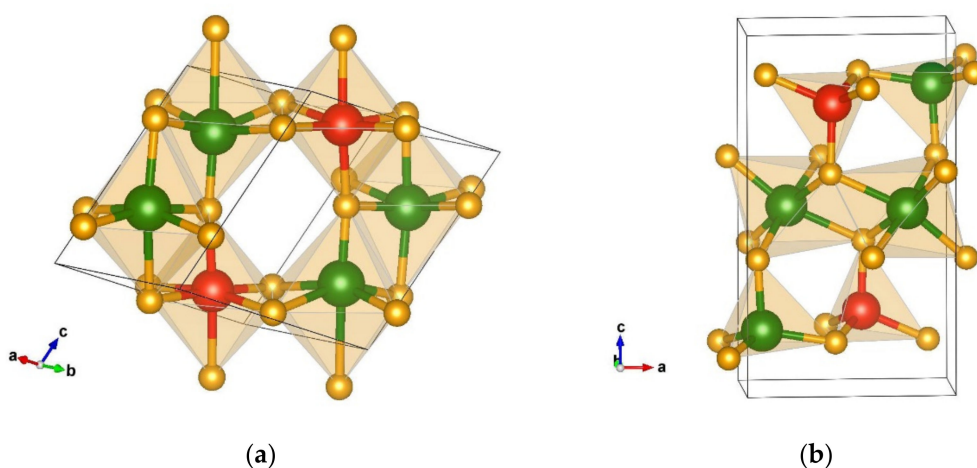


Figure 2. Visualization of favorable Cr₂SiN₄ modifications: (a) δ -Cr₂SiN₄-type in space group *P21/m* (no. 11). (b) ϵ -Cr₂SiN₄-type in space group *P21/m* (no. 11). Green, red, and yellow spheres denote Cr, Si, and N atoms, respectively.

One more energetically favorable candidate is a monoclinic structure, denoted as ϵ -Cr₂SiN₄-type, which appears in space group *P21/m* (no. 11). It is visualized in Figure 2b with the unit cell parameters a = 5.09, b = 2.89, c = 8.90 Å, and $\beta = 90.20$. However, the ϵ -Cr₂SiN₄-type is composed of SiN₄ tetrahedra (with interatomic distances 1 × 1.77 Å-N, 2 × 1.72 Å-N, and 1 × 1.73 Å-N), while chromium is four-fold and six-fold coordinated by nitrogen, thus, forming CrN₄ tetrahedra and CrN₆ octahedra (interatomic distances

are Cr(1) $1 \times 1.90 \text{ \AA-N}$, $4 \times 2.00 \text{ \AA-N}$, $1 \times 2.07 \text{ \AA-N}$, Cr(2) $1 \times 1.75 \text{ \AA-N}$, $2 \times 1.78 \text{ \AA-N}$, and $1 \times 1.82 \text{ \AA-N}$). Apart from being the same space group as the δ -phase, the monoclinic ε -modification resembles more the α - and β -Cr₂SiN₄-types (Tables 1 and 2 and Figure 2).

Two other interesting favorable structure candidates are monoclinic modifications belonging to space group Pm (no. 6) and are visualized in Figure 3a,b, respectively. The first one (a) is denoted the λ -Cr₂SiN₄-type with unit cell parameters $a = 5.07$, $b = 2.88$, $c = 9.27 \text{ \AA}$, and $\beta = 99.77$, while the other one (b) is called the λ' -Cr₂SiN₄-type and has the unit cell parameters $a = 5.06$, $b = 2.87$, $c = 9.18 \text{ \AA}$, and $\beta = 90.97$. These two structures are structurally and energetically very similar, and both of them are composed of CrN₄ and SiN₄ tetrahedra, with CrN₆ octahedra between them.

The CrN₆ octahedra are edge-connected, with corner-connected tetrahedra. Similar to the previous structures of the α -, β -, ε -Cr₂SiN₄-type of modifications, these tetrahedra have the opposite orientations in different layers of the structure. In the λ -Cr₂SiN₄-type of structure, chromium is connected to nitrogen with atom–atom distances Cr(1) $1 \times 1.70 \text{ \AA-N}$, $2 \times 1.79 \text{ \AA-N}$, $1 \times 1.89 \text{ \AA-N}$, Cr(2) $1 \times 1.91 \text{ \AA-N}$, $2 \times 1.93 \text{ \AA-N}$, $2 \times 2.02 \text{ \AA-N}$, $1 \times 2.19 \text{ \AA-N}$, Cr(3) $1 \times 1.91 \text{ \AA-N}$, $2 \times 1.93 \text{ \AA-N}$, $3 \times 2.09 \text{ \AA-N}$, Cr(4) $2 \times 1.75 \text{ \AA-N}$, $1 \times 1.79 \text{ \AA-N}$, $1 \times 1.81 \text{ \AA-N}$, and $1 \times 2.64 \text{ \AA-N}$, while there are also two different types of SiN₄ tetrahedra (with interatomic distances Si(1) $1 \times 1.72 \text{ \AA-N}$, $1 \times 1.76 \text{ \AA-N}$, $2 \times 1.73 \text{ \AA-N}$, Si(2) $3 \times 1.74 \text{ \AA-N}$, and $1 \times 1.75 \text{ \AA-N}$).

The modification referred to as λ' -Cr₂SiN₄-type has a similar structure, with chromium being tetrahedrally and octahedrally coordinated by nitrogen in four different ways (with atom–atom distances Cr(1) $2 \times 1.75 \text{ \AA-N}$, $1 \times 1.80 \text{ \AA-N}$, $1 \times 1.81 \text{ \AA-N}$, Cr(2) $1 \times 1.92 \text{ \AA-N}$, $2 \times 1.94 \text{ \AA-N}$, $2 \times 2.01 \text{ \AA-N}$, $1 \times 2.23 \text{ \AA-N}$, Cr(3) $1 \times 1.92 \text{ \AA-N}$, $2 \times 1.97 \text{ \AA-N}$, $2 \times 2.01 \text{ \AA-N}$, $1 \times 2.08 \text{ \AA-N}$, Cr(4) $1 \times 1.71 \text{ \AA-N}$, $2 \times 1.78 \text{ \AA-N}$, and $1 \times 1.88 \text{ \AA-N}$) and two types of SiN₄ tetrahedra (interatomic distances Si(1) $1 \times 1.73 \text{ \AA-N}$, $2 \times 1.74 \text{ \AA-N}$, $1 \times 1.75 \text{ \AA-N}$, Si(2) $2 \times 1.74 \text{ \AA-N}$, and $2 \times 1.73 \text{ \AA-N}$).

We note that, after optimization on the *ab-initio* level with the LDA-PZ functional and with the GGA-PBE functional, both structures remain distinct but stay in the same space group.

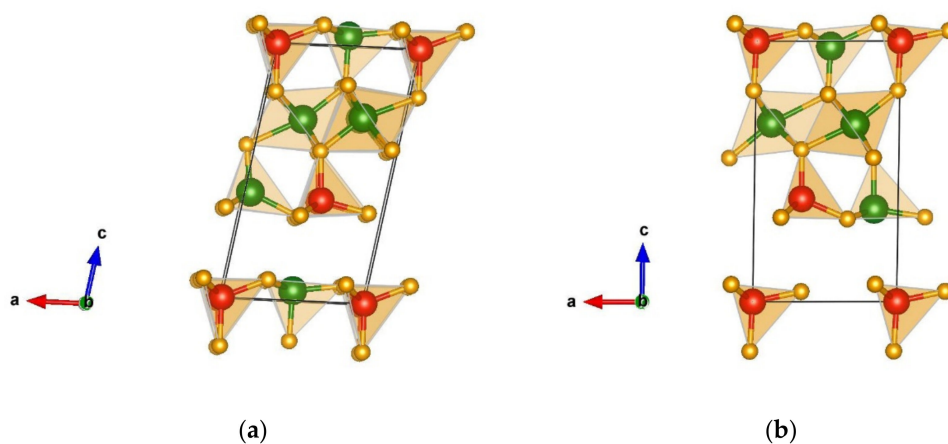


Figure 3. Visualization of favorable Cr₂SiN₄ modifications found in space group Pm (no. 6): (a) λ -Cr₂SiN₄-type; (b) λ' -Cr₂SiN₄-type. Green, red, and yellow spheres denote Cr, Si, and N atoms, respectively.

3.1.2. Structural Details of Non-Favorable Structures Found after a Global Search

At extreme conditions of temperature and/or pressure, the global optimization (GO) yielded several additional candidate structures, and Table 3 presents the structural data for the five energetically non-favorable yet structurally promising GO modifications. The first modification, lowest in the energy compared to the other structures within this group is denoted as *nf1*-Cr₂SiN₄-type and appears in space group $P21/m$ (no. 11). It is visualized in Figure 4a with the unit cell parameters $a = 5.03$, $b = 2.89$, $c = 9.25 \text{ \AA}$, and $\beta = 100.34$.

It is composed of CrN_6 octahedra positioned between two layers of nitrogen tetrahedra coordinating silicon and chromium. Hence, chromium in this structure has a four-fold as well as a six-fold coordination (with atom–atom distances $\text{Cr}(1)$ $1 \times 1.94 \text{ \AA-N}$, $2 \times 1.98 \text{ \AA-N}$, $2 \times 2.00 \text{ \AA-N}$, $1 \times 2.08 \text{ \AA-N}$, $\text{Cr}(2)$ $3 \times 1.77 \text{ \AA-N}$, $1 \times 1.80 \text{ \AA-N}$, and $1 \times 2.72 \text{ \AA-N}$) while silicon still remains in four-fold coordination (with the interatomic distances $1 \times 1.76 \text{ \AA-N}$ and $3 \times 1.74 \text{ \AA-N}$). Both CrN_4 and SiN_4 tetrahedra in the upper and lower part of the structure are oriented in the opposite directions.

The next modification according to the total energy ranking is referred to as *nf2*- Cr_2SiN_4 -type and crystallizes in space group *Cc* (no. 9). It is visualized in Figure 4b with the unit cell parameters $a = 5.06$, $b = 14.14$, $c = 4.77 \text{ \AA}$, and $\beta = 121.05$. Within this structure, chromium is five-fold coordinated by nitrogen and forms two types of polyhedra (with atom–atom distances $\text{Cr}(1)$ $1 \times 1.84 \text{ \AA-N}$, $1 \times 1.87 \text{ \AA-N}$, $1 \times 1.88 \text{ \AA-N}$, $1 \times 1.91 \text{ \AA-N}$, $1 \times 1.93 \text{ \AA-N}$, $\text{Cr}(2)$ $1 \times 1.78 \text{ \AA-N}$, $1 \times 1.79 \text{ \AA-N}$, $1 \times 1.84 \text{ \AA-N}$, $1 \times 2.00 \text{ \AA-N}$, and $1 \times 2.11 \text{ \AA-N}$) while silicon is four-fold coordinated by nitrogen (interatomic distances are $1 \times 1.71 \text{ \AA-N}$, $1 \times 1.77 \text{ \AA-N}$, $1 \times 1.75 \text{ \AA-N}$, and $1 \times 1.76 \text{ \AA-N}$).

Other relevant modifications are denoted as *nf3*- Cr_2SiN_4 -type, *nf4*- Cr_2SiN_4 -type, and *nf5*- Cr_2SiN_4 -type with the first two structures appearing in the space group *Pm* (no. 6) and the last one showing space group *P-1* (no. 2), respectively. The total energies of these five modifications on ab initio level (GGA-PBE functional) are listed in Table 1. Furthermore, we note that most of the energetically favorable and non-favorable structures found after global optimization exhibit low symmetry, mostly orthorhombic and monoclinic symmetry (Tables 2 and 3). This is in agreement with previous theoretical reports in the closely related Si_3N_4 chemical system, where orthorhombic and monoclinic structures have been proposed [69].

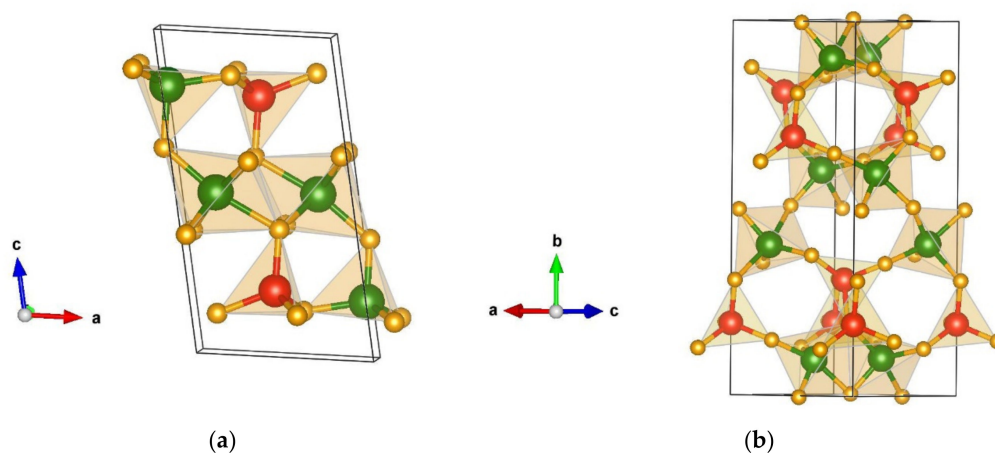


Figure 4. Visualization of non-favorable Cr_2SiN_4 modifications: (a) *nf1*- Cr_2SiN_4 -type in space group *P21/m* (no. 11); (b) *nf2*- Cr_2SiN_4 -type in space group *Cc* (no. 9). Green, red, and yellow spheres denote Cr, Si, and N atoms, respectively.

Table 3. The modifications, space groups, unit cell parameters, and atomic positions for non-favorable Cr_2SiN_4 modifications found using global optimization and later optimized at the GGA-PBE level of calculation.

Modifications and Space Group	Cell Parameters	Position of Atoms
<i>nf1</i> - Cr_2SiN_4 -type <i>P21/m</i> No 11	$a = 5.03$ $b = 2.89$ $c = 9.25$ $\beta = 100.34$	Cr 0.780740 0.750000 0.501443
		Cr 0.025858 0.250000 0.824580
		Si 0.517842 0.750000 0.797882
		N 0.959527 0.250000 0.630184
		N 0.552291 0.250000 0.393501
		N 0.609701 0.750000 0.135709
N 0.136923 0.250000 0.122932		

Table 3. Cont.

Modifications and Space Group	Cell Parameters	Position of Atoms
<i>nf2</i> -Cr ₂ SiN ₄ -type <i>Cc</i> No 9	a = 5.06 b = 14.14 c = 4.77 β = 121.05	Cr 0.622331 0.095134 0.360180
		Cr 0.380879 0.098904 0.725602
		Si 0.000000 0.191719 0.000000
		N 0.487148 0.004091 0.555289
		N 0.511786 0.374204 0.196387
		N 0.720274 0.147401 0.064041
<i>nf3</i> -Cr ₂ SiN ₄ -type <i>Pm</i> No 6	a = 6.79 b = 3.09 c = 6.88 β = 109.29	Cr 0.319643 0.500000 0.397294
		Cr 0.308694 0.500000 0.793094
		Cr 0.034585 0.000000 0.406174
		Cr 0.733922 0.500000 0.593240
		Si 0.000000 0.000000 0.000000
		Si 0.588865 0.000000 0.169164
		N 0.515186 0.500000 0.666342
		N 0.819399 0.000000 0.531146
		N 0.551036 0.500000 0.283640
		N 0.215615 0.000000 0.242977
		N 0.384133 0.000000 0.929487
		N 0.000403 0.500000 0.870324
N 0.122011 0.500000 0.540245		
N 0.829057 0.000000 0.140470		
<i>nf4</i> -Cr ₂ SiN ₄ -type <i>Pm</i> No 6	a = 7.37 b = 3.05 c = 7.56 β = 115.96	Cr 0.779088 0.000000 0.218259
		Cr 0.459516 0.500000 0.327876
		Cr 0.253478 0.000000 0.544973
		Cr 0.396471 0.500000 0.935322
		Si 0.000000 0.500000 0.000000
		Si 0.852505 0.000000 0.603621
		N 0.330961 0.500000 0.474928
		N 0.889506 0.500000 0.738026
		N 0.613308 0.000000 0.401256
		N 0.355218 0.000000 0.802744
		N 0.932400 0.000000 0.070113
		N 0.262965 0.500000 0.082041
N 0.643042 0.500000 0.129399		
N 0.988794 0.000000 0.464379		
<i>nf5</i> -Cr ₂ SiN ₄ -type <i>P-1</i> No 2	a = 7.17 b = 3.06 c = 7.41 α = 89.69 β = 66.68 γ = 88.06	Cr 0.654478 0.292004 0.523373
		Cr 0.288987 0.742844 0.838266
		Si 0.865354 0.748679 0.767528
		N 0.255163 0.244316 0.972502
		N 0.804235 0.255276 0.687399
		N 0.477326 0.210250 0.368818
N 0.127792 0.732554 0.709190		

3.2. Data Mining (DM) Based Searches Using the ICSD Database

The DM-based searches were performed within the ICSD database, which, in the latest release contains 242,828 inorganic structures, out of which more than 80% have already been assigned to distinct structure types (up to now, 9724 structure types are listed in the ICSD) [44,45]. Using the final prototype criterion as part of the KDD approach [46–48] to eliminate quasi-duplicate structures, the number of structures was reduced to 66 unique structure candidates in the *A1B2C4* chemical system. After performing full structural optimization on the ab initio level, the number of structure candidates was further reduced. Table 4 shows the total energy ranking of the DM-based structure candidates in the Cr₂SiN₄ system using the GGA-PBE functional.

Full structural data for all Cr_2SiN_4 modifications found from the DM-based searches are presented in Table 5, while their corresponding total energies are listed in Table 4. The data-mining-based searches of the ICSD database resulted in many possible modifications, among which the four structures presented here are distinguished as being the energetically most favorable ones, while the others corresponded to non-favorable DM structure candidates.

Table 4. The total energy and relative energy values compared to the global minimum (spinel structure taken as the zero of energy) of Cr_2SiN_4 modifications obtained from DM-based searches and calculated using GGA-PBE.

Modification	Total Energy (Eh)	Relative Energy (kcal/mol)
Al_2MgO_4 -spinel-type	−5193.507	0.0
Na_2MnCl_4 -type	−5193.436	44.553
TiMn_2O_4 -type	−5193.414	58.358
Mg_2SiO_4 -type	−5193.403	65.261
Ca_2RuO_4 -type	−5193.402	65.889
HgC_2O_4 -like	−5193.400	67.144
Ca_2IrO_4 -type	−5193.349	99.147
CaB_2O_4 -like	−5193.347	100.402
Mn_2SnS_4 -type	−5193.342	103.539

Table 5. The modifications, space groups, unit cell parameters, and atomic positions for Cr_2SiN_4 modifications obtained from data-mining-based searches and local optimization at the GGA-PBE level.

Modifications and Space Group	Cell Parameters	Position of Atoms
Al_2MgO_4 -spinel-type <i>Fd-3m</i> No 227	a = 7.88	Cr 0.000000 0.000000 0.000000
		Si 0.625000 0.625000 0.625000
		N 0.752483 0.752483 0.752483
Na_2MnCl_4 -type <i>Pbam</i> No 55	a = 4.74 b = 8.70 c = 2.73	Cr 0.433387 0.175989 0.500000
		Si 0.000000 0.000000 0.000000
		N 0.133667 0.203146 0.000000
		N 0.256351 0.966597 0.500000
TiMn_2O_4 -type <i>P4322</i> No 95	a = 5.64 c = 7.74	Cr 0.500000 0.288490 0.000000
		Cr 0.234522 0.234522 0.625000
		Si 0.000000 0.259306 0.000000
		N 0.239859 0.499775 0.998379
		N 0.246452 0.027106 0.010564
Mg_2SiO_4 -type <i>Pnma</i> No 62	a = 9.42 b = 5.45 c = 4.82	Cr 0.500000 0.500000 0.500000
		Cr 0.751225 0.750000 0.005741
		Si 0.911733 0.750000 0.580414
		N 0.915086 0.750000 0.227101
		N 0.579248 0.750000 0.754925
		N 0.831733 0.498905 0.747339
Ca_2RuO_4 -type <i>Pbca</i> No 61	a = 4.55 b = 4.88 c = 10.32	Cr 0.951271 0.088328 0.314395
		Si 0.000000 0.000000 0.000000
		N 0.189814 0.299961 0.071415
		N 0.821277 0.910789 0.170556

Table 5. Cont.

Modifications and Space Group	Cell Parameters	Position of Atoms
HgC ₂ O ₄ -like <i>P21</i> No 4	a = 5.34 b = 5.09 c = 5.36 β = 115.62	Cr 0.009785 0.463302 0.266681
		Cr 0.242643 0.853311 0.472408
		Si 0.651871 0.000000 0.959796
		N 0.021251 0.353294 0.916553
		N 0.626651 0.296871 0.103741
		N 0.597719 0.030584 0.610720
Ca ₂ IrO ₄ -type <i>P-62m</i> No 189	a = 8.33 c = 2.70	Cr 0.000000 0.000000 0.000000
		Cr 0.333333 0.666667 0.500000
		Cr 0.699230 0.000000 0.500000
		Si 0.337748 0.000000 0.000000
		N 0.173727 0.000000 0.500000
		N 0.473996 0.000000 0.500000
CaB ₂ O ₄ -like <i>Pccn</i> No 56	a = 7.98 b = 14.42 c = 4.85	Cr 0.931376 0.565538 0.393557
		Cr 0.170647 0.535703 0.989804
		Si 0.857355 0.679567 0.867484
		N 0.864237 0.698217 0.499220
		N 0.303715 0.441717 0.754883
		N 0.009972 0.618966 0.076401
Mn ₂ SnS ₄ -type <i>Cmmm</i> No 65	a = 5.58 b = 7.82 c = 2.76	Cr 0.750000 0.750000 0.500000
		Si 0.000000 0.000000 0.000000
		N 0.000000 0.247324 0.000000
		N 0.220861 0.000000 0.500000

3.2.1. Structural Analysis of Low-Energy Candidates from the DM-Based Searches

The Al₂MgO₄-spinel-type modification [70,71], generated from the DM-based searches and visualized in Figure 5a, is the lowest one in the calculated total energy at both the GGA-PBE and the LDA-PZ level, for the whole energy landscape including the structures obtained from the GO and the PCAE method calculations. It exhibits space group *Fd-3m* (no. 227) with unit cell parameters a = 7.88 Å at the GGA-PBE level of calculation with all structural data presented in Table 5.

In the Al₂MgO₄-type modification, chromium is six-fold coordinated forming a CrN₆ octahedron with the interatomic distance Cr 6 × 1.95 Å-N, while silicon is four-fold coordinated forming a SiN₄ tetrahedron with the atom–atom distance 4 × 1.74 Å-N. In this cubic modification, the CrN₆ octahedra are connected by edges while the SiN₄ tetrahedra are corner-connected. When performing structure optimizations of the candidates on the DFT-LDA level, the Al₂MgO₄-spinel-type modification remains the global minimum (Tables A1 and A2). We note that the Al₂MgO₄-spinel-type of the structure appears in more than 4000 compounds (4250) with the chemical formula A1B2C4 indicating the importance of this structure-type on the energy landscape of ternary systems [44,45].

The next favorable modification found after DM is in the Na₂MnCl₄-type [72], which is an orthorhombic structure that appears in space group *Pbam* (no. 55) with unit cell parameters a = 4.73, b = 8.70, and c = 2.73 Å and is visualized in Figure 5b. In this modification, both chromium and silicon are six-fold coordinated by nitrogen, thus, forming distorted octahedra that are quite different from each other.

The CrN₆ octahedra are quite similar to those in the WC structure-type, while the SiN₆ octahedra are “NaCl-type” octahedra. Interatomic distances in the CrN₆ octahedra are longer (1 × 1.92 Å-N, 2 × 1.97 Å-N, 2 × 1.98 Å-N, and 1 × 2.01 Å-N) than in the SiN₆ octahedra (4 × 1.85 Å-N, 2 × 1.88 Å-N). The SiN₆ octahedra are positioned in the center

and at the edges of the cell, with the CrN_6 octahedra connecting them. Both edge and corner connections are observed.

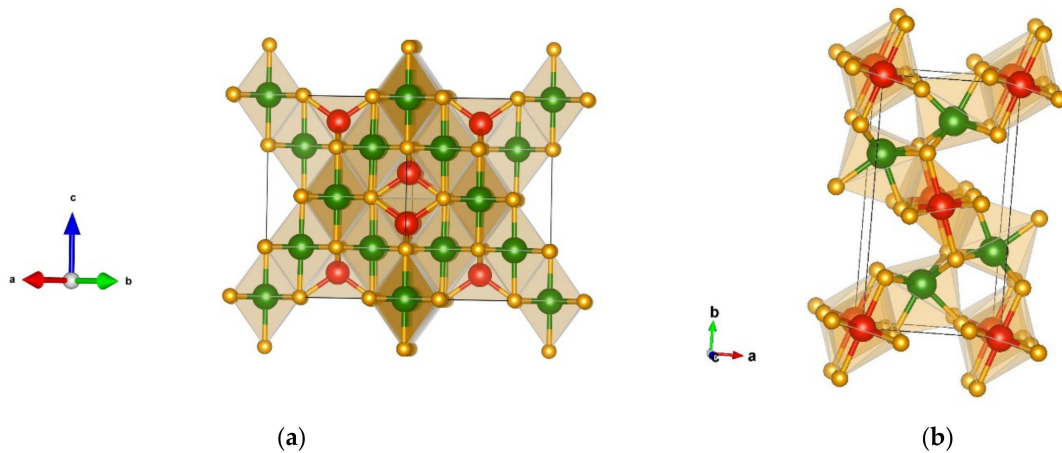


Figure 5. Visualization of favorable Cr_2SiN_4 modifications: (a) Al_2MgO_4 -spinel-type in space group $Fd\bar{3}m$ (no. 227); (b) Na_2MnCl_4 -type that appears in space group $Pbam$ (no. 55). Green, red, and yellow spheres denote Cr, Si, and N atoms, respectively.

The next favorable modification obtained via DM is denoted as TiMn_2O_4 -type [73]. It is a tetragonal structure in space group $P4322$ (no.95) with unit cell parameters $a = 5.64$ and $c = 7.74$ Å and is visualized in Figure 6a. In the TiMn_2O_4 phase, chromium is both four-fold and six-fold coordinated by nitrogen, thus, forming CrN_4 tetrahedra (with atom–atom distances 2×1.78 Å–N and 2×1.81 Å–N) and CrN_6 octahedra (with atom–atom distances 2×1.89 Å–N, 2×1.97 Å–N, and 2×2.05 Å–N). Silicon is six-fold coordinated by nitrogen with interatomic distances (2×1.86 Å–N and 4×1.91 Å–N). The octahedra are edge-connected, while the CrN_4 tetrahedra are corner-connected.

The next modification obtained from the data mining search is a structure denoted as Mg_2SiO_4 - (Forsterite) type of structure [74], and it crystallizes in space group $Pnma$ (no. 62) with unit cell parameters $a = 9.42$, $b = 5.45$, and $c = 4.82$ Å. Within this modification, two types of CrN_6 octahedra are connected by edges and oriented in the structure in two directions with interatomic distances (Cr(1) 2×1.92 Å–N, 2×1.98 Å–N, 2×2.00 Å–N, Cr(2) 1×1.88 Å–N, 2×1.95 Å–N, 2×2.00 Å–N, and 1×2.02 Å–N). Silicon is four-fold coordinated by nitrogen (with atom–atom distances 1×1.70 Å–N, 2×1.76 Å–N, and 1×1.77 Å–N) connected by the edges; the structure is visualized in Figure 6b.

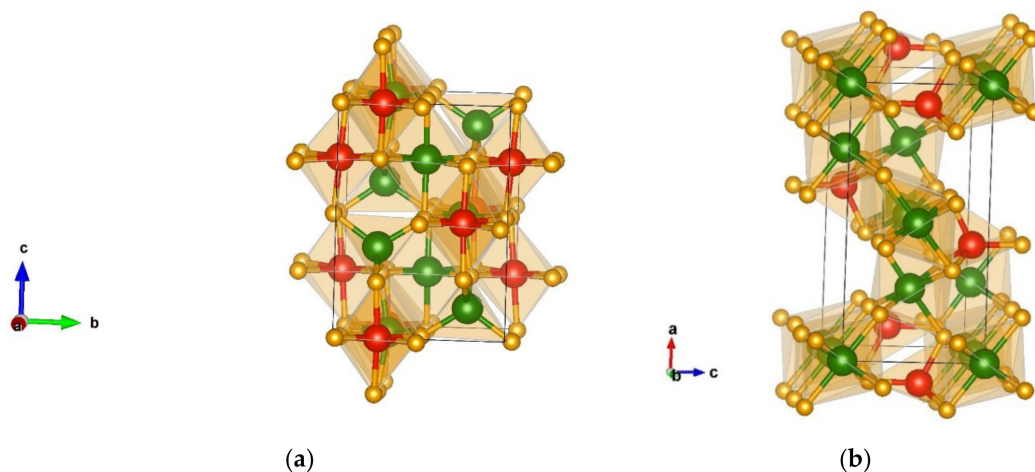


Figure 6. Visualization of favorable Cr_2SiN_4 modifications: (a) TiMn_2O_4 -type in space group $P4322$ (no. 95); (b) Mg_2SiO_4 -type in space group $Pnma$ (no.62). Green, red, and yellow spheres denote Cr, Si, and N atoms, respectively.

3.2.2. Structural Analysis of Non-Favorable Candidates Found after Data Mining

The first non-favorable energy minimum found after data mining appears in the Ca_2RuO_4 -type [75] and is visualized in Figure 7a. This is an orthorhombic structure that appears in space group $Pbca$ (no. 61) with the unit cell parameters $a = 4.55$, $b = 4.88$, and $c = 10.31$ Å. Chromium and silicon are both six-fold coordinated by nitrogen but form different octahedra. Similar to the energetically favorable Na_2MnCl_4 -type modification, within this modification, the CrN_6 octahedra resemble those in the WC-type of structure with the interatomic distances 1×1.82 Å-N, 1×1.89 Å-N, 1×1.90 Å-N, 1×1.94 Å-N, 1×1.97 Å-N, and 1×2.49 Å-N.

These octahedra are connected by edges to each other; however, the connection to the SiN_6 octahedra is via edges and corners as well. The whole structure consists of layers of different octahedra, where the SiN_6 ones are located on the faces and in the center of the cell with the CrN_6 octahedra situated in-between.

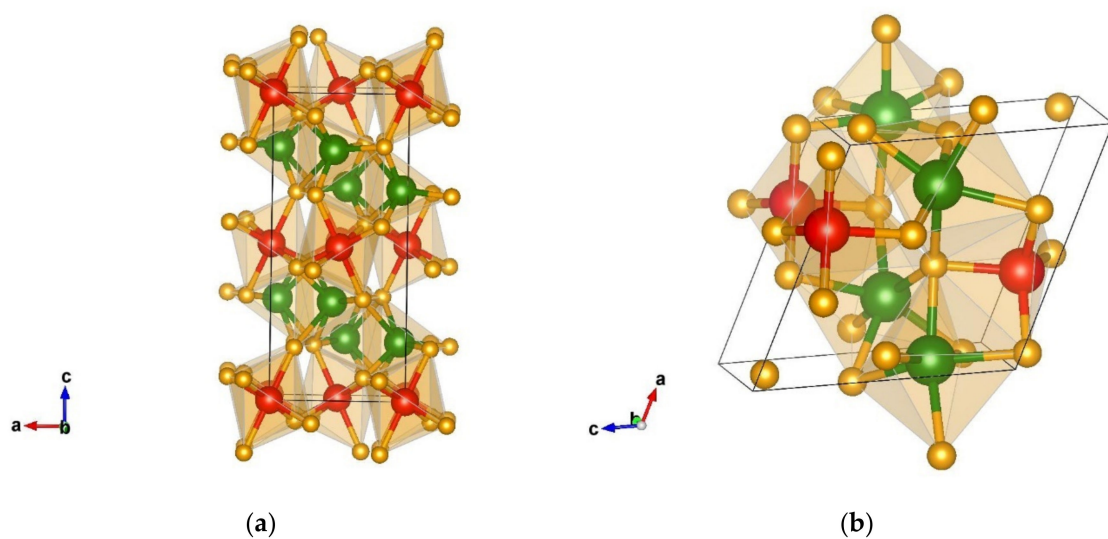


Figure 7. Visualization of non-favorable Cr_2SiN_4 modification from data-mining: (a) Ca_2RuO_4 -type in space group $Pbca$ (no. 61), (b) HgC_2O_4 -type in space group $P21$ (no. 4).

The next non-favorable modification found after data mining is denoted as a HgC_2O_4 -like type of structure and crystallizes in space group $P21$ (no. 4). We note that the starting HgC_2O_4 structure [76] after DFT optimization has been structurally modified, however, within the same space group (no.4), thus, resulting in a HgC_2O_4 -like structure. This is a monoclinic structure with the unit cell parameters $a = 5.34$, $b = 5.09$, $c = 5.36$, and $\beta = 115.62$, with the structural parameters with corresponding energies given in Tables 4 and 5.

Within this structure, chromium is six-fold coordinated by nitrogen forming CrN_6 octahedra (atom–atom distance Cr(1) 1×1.83 Å-N, 1×1.88 Å-N, 1×1.94 Å-N, 1×1.98 Å-N, 1×2.03 Å-N, 1×2.19 Å-N, Cr(2) 1×1.91 Å-N, 1×1.94 Å-N, 1×1.95 Å-N, 1×1.99 Å-N, 1×2.00 Å-N, and 1×2.09 Å-N), connected by faces and corners among each other. Silicon is four-fold coordinated forming edge- and corner-connected SiN_4 tetrahedra with the interatomic distances 1×1.72 Å-N, 1×1.73 Å-N, 1×1.75 Å-N, and 1×1.77 Å-N. The structure is visualized in Figure 7b.

The next modification by energy shows a Ca_2IrO_4 -type [77] structure; it exhibits the space group $P-62m$ (no. 189) with the unit cell parameters $a = 8.33$ and $c = 2.70$ and is visualized in Figure 8a. Within the structure, chromium is six-fold and seven-fold coordinated by nitrogen with the interatomic distances Cr(1) 6×1.98 Å-N, Cr(2) 6×2.08 Å-N, 3×2.42 Å-N, Cr(3) 1×1.88 Å-N, 4×2.02 Å-N, and 2×2.18 Å-N. The CrN_6 octahedra are face-connected resembling the ones in the WC-type of a structure, while the CrN_7 polyhedra are edge- and corner-connected. Similarly, the SiN_6 octahedra are edge-

and corner-connected, with the atom–atom distances $2 \times 1.76 \text{ \AA-N}$, $2 \times 1.79 \text{ \AA-N}$, and $2 \times 1.92 \text{ \AA-N}$.

Another interesting modification obtained from the data mining search is the orthorhombic structure denoted as a CaB_2O_4 -like structure, visualized in Figure 8b. This modification crystallizes in space group $Pccn$ (no. 56) with the unit cell parameters $a = 7.98$, $b = 14.42$, and $c = 4.85$. Similarly, as with the HgC_2O_4 -like modification, the CaB_2O_4 -like structure is modified during the local optimization from the original prototypic CaB_2O_4 structure [78] but still within the same space group (no. 56).

In this structure, chromium is five-fold and six-fold coordinated by nitrogen forming two different polyhedra with the atom–atom distances Cr(1) $1 \times 1.83 \text{ \AA-N}$, $1 \times 1.87 \text{ \AA-N}$, $1 \times 1.98 \text{ \AA-N}$, $1 \times 1.99 \text{ \AA-N}$, $1 \times 2.01 \text{ \AA-N}$, $1 \times 2.05 \text{ \AA-N}$, Cr(2) $1 \times 1.81 \text{ \AA-N}$, $1 \times 1.82 \text{ \AA-N}$, $1 \times 1.88 \text{ \AA-N}$, $1 \times 1.92 \text{ \AA-N}$, and $1 \times 2.07 \text{ \AA-N}$, and one has a SiN_5 polyhedron with the interaction distances $2 \times 1.81 \text{ \AA-N}$, $1 \times 1.88 \text{ \AA-N}$, and $2 \times 1.90 \text{ \AA-N}$.

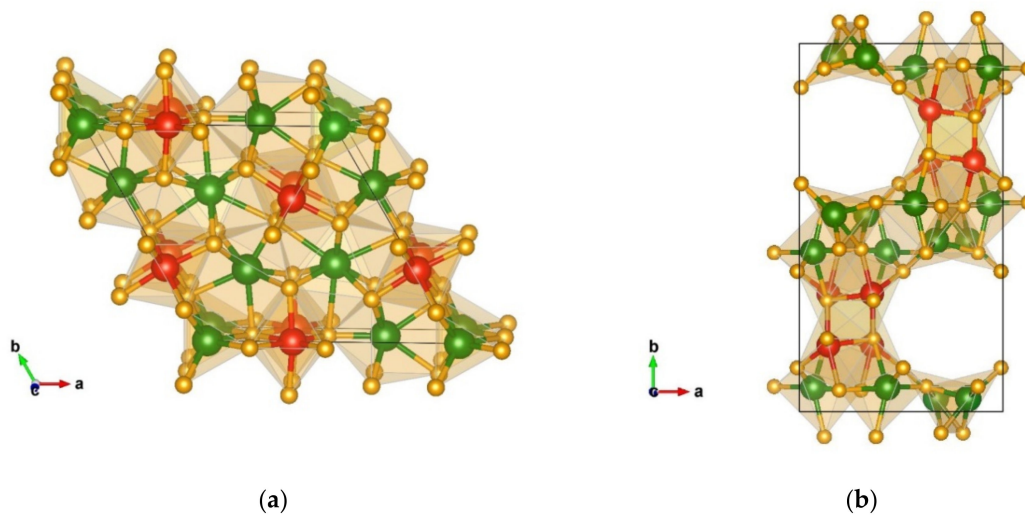


Figure 8. Visualization of non-favorable Cr_2SiN_4 modifications obtained from data-mining: (a) Ca_2IrO_4 -type in space group $P-62m$ (no. 189); (b) CaB_2O_4 -type in space group $Pccn$ (no. 56). Green, red, and yellow spheres denote Cr, Si, and N atoms, respectively.

A final interesting modification from the data mining search is denoted as Mn_2SnS_4 -type [79] and is visualized in Figure 9. This orthorhombic structure appears in the space group $Cmmm$ (no. 65) with the unit cell parameters $a = 5.58$, $b = 7.82$, and $c = 2.76$. In this structure, both chromium and silicon, are six-fold coordinated by nitrogen with edge-connected octahedra and the interatomic distances Cr $6 \times 1.96 \text{ \AA-N}$, Si $4 \times 1.85 \text{ \AA-N}$, and $2 \times 1.93 \text{ \AA-N}$.

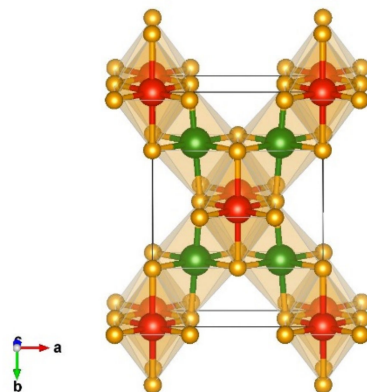


Figure 9. Visualization of non-favorable Cr_2SiN_4 modification obtained from data-mining referred to as Mn_2SnS_4 -type in space group $Cmmm$ (no 65).

We note that most of the structure candidates found using DM-based searches show orthorhombic symmetry (Table 5), in some cases reminiscent of the structurally related Si_3N_4 chemical system where orthorhombic structures have also been found [69]. In this context, we would like to remark on the Cu_2HgI_4 type of structure [80]. This structure type has been recently predicted to exist as a modification in a study of novel hard phases of Si_3N_4 [69].

The same Cu_2HgI_4 type has also been found in our DM-based searches; however, it is energetically much worse than most of the other DM or GO/PCAE-based structure candidates ($E_{\text{tot}} = -5193.312 \text{ Eh}$ calculated using the GGA-PBE functional). Full structural optimization resulted in the original prototypic structure in tetragonal space group $I-42m$ (no. 121) with unit cell parameters $a = 4.34$ and $c = 8.09 \text{ \AA}$, at the GGA-PBE level of computation (both chromium and silicon are fourfold coordinated by nitrogen forming tetrahedra with interatomic distances of $\text{Cr } 4 \times 1.80 \text{ \AA-N}$ and $\text{Si } 4 \times 1.75 \text{ \AA-N}$).

3.3. Structural Searches Using the PCAE Method

Finally, the Primitive Cell approach for Atom Exchange (PCAE) method was employed for generating alternative structure candidates in the Cr_2SiN_4 compound, starting from typical structures in the related Si_3N_4 system, the γ -, β -, and α -phase of Si_3N_4 . Ranking the ab initio minimized structures according to the calculated total energy using the GGA-PBE functional, the most promising candidates generated using the PCAE method are presented in Table 6.

Table 6. The total energy and relative energy values compared to the global minimum (spinel structure taken as the zero of the energy) of Cr_2SiN_4 modifications found using the PCAE method and locally optimized using the GGA-PBE functional.

Modification	Total Energy (Eh)	Relative Energy (kcal/mol)
γ - Cr_2SiN_4 -type	-5193.435	45.181
Cr_2SiN_4 -PCAE-1-type	-5193.385	76.556
Cr_2SiN_4 -PCAE-2-type	-5193.374	83.459

Structural Details of Candidates Found Using the PCAE Method

The lowest energy minimum found using the PCAE method was denoted the γ - Cr_2SiN_4 -type modification. Figure 10a shows a prototypic γ -phase in the Si_3N_4 system [71], which was used as starting structure for generating the γ - Cr_2SiN_4 -type. The Si_3N_4 γ -phase crystallizes in the cubic space group $I-43d$ (no. 220), [71] forming corner connected tetrahedra of silicon atoms (Figure 10a). However, after local optimization in the Cr_2SiN_4 system using both GGA-PBE and LDA-PZ functionals, it converts to the γ - Cr_2SiN_4 -type modification. It is a low-energy candidate in the Cr_2SiN_4 system; however, it is structurally completely different from the starting γ -phase in the Si_3N_4 system (compare Figure 10a,b).

The γ - Cr_2SiN_4 -type modification crystallizes in the monoclinic space group Cc (no. 9) with unit cell parameters $a = 5.62$, $b = 8.96$, $c = 5.36 \text{ \AA}$, and $\beta = 117.93$, with both cations—chromium and silicon—being six-fold coordinated by nitrogen where these octahedra are edge- and face-connected (Figure 10b). We deal with two different types of CrN_6 octahedra with the interatomic distances $\text{Cr}(1) 1 \times 1.84 \text{ \AA-N}$, $1 \times 1.85 \text{ \AA-N}$, $1 \times 1.92 \text{ \AA-N}$, $1 \times 1.96 \text{ \AA-N}$, $1 \times 2.01 \text{ \AA-N}$, $1 \times 2.13 \text{ \AA-N}$, $\text{Cr}(2) 1 \times 1.83 \text{ \AA-N}$, $1 \times 1.90 \text{ \AA-N}$, $1 \times 1.92 \text{ \AA-N}$, $1 \times 1.96 \text{ \AA-N}$, $1 \times 2.01 \text{ \AA-N}$, and $1 \times 2.03 \text{ \AA-N}$; the atom–atom distances in the SiN_6 octahedra are $1 \times 1.74 \text{ \AA-N}$, $1 \times 1.75 \text{ \AA-N}$, $1 \times 1.81 \text{ \AA-N}$, $1 \times 2.08 \text{ \AA-N}$, $1 \times 2.20 \text{ \AA-N}$, and $1 \times 2.34 \text{ \AA-N}$). In the closely related Si_3N_4 compound, there has been a prediction of novel monoclinic phases from first-principles calculations [69].

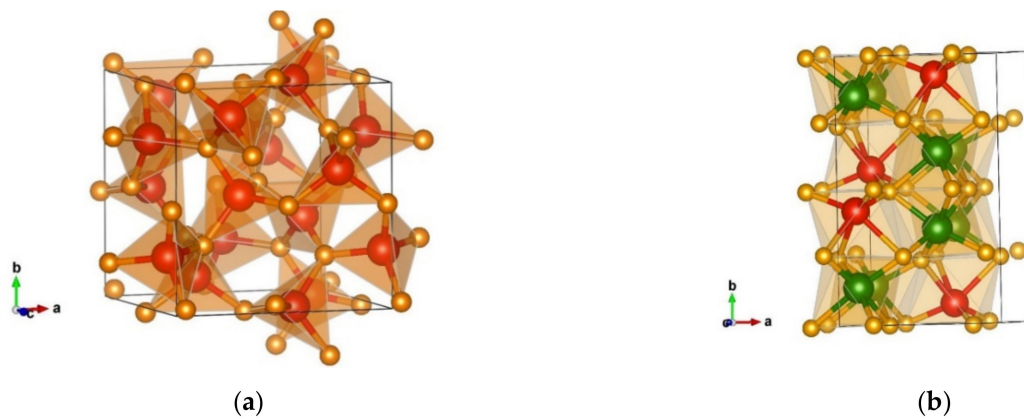


Figure 10. Visualization of: (a) the Si_3N_4 γ -phase in space group $I-43d$ (no. 220); (b) γ - Cr_2SiN_4 -type in space group Cc (no. 9). Green, red, and yellow spheres denote Cr, Si, and N atoms, respectively.

The next minimum found using the PCAE method is marked as Cr_2SiN_4 -PCAE-1 phase, which is energetically less favorable than the γ -phase (Table 6). The Cr_2SiN_4 -PCAE-1 type has been generated similarly to the previous one, starting from the β -phase of Si_3N_4 in the hexagonal $P63/m$ (no. 176) space group [81,82]. After ab initio structural optimization in the Cr_2SiN_4 system, the structure converted to a monoclinic modification denoted Cr_2SiN_4 -PCAE-1 that crystallizes in space group Pm (no. 6) with unit cell parameters $a = 7.04465$, $b = 3.03610$, $c = 7.03270$, $\beta = 110.7203$ (Table 7).

In this structure type, both chromium and silicon are four-fold and five-fold coordinated by nitrogen forming different types of polyhedra (Figure 11a). There are two different CrN_4 tetrahedra and two different CrN_5 polyhedra, with the atom–atom distances Cr(1) $2 \times 1.86 \text{ \AA-N}$, $1 \times 1.89 \text{ \AA-N}$, $1 \times 1.95 \text{ \AA-N}$, $1 \times 2.01 \text{ \AA-N}$, Cr(2) $2 \times 1.81 \text{ \AA-N}$, $1 \times 1.88 \text{ \AA-N}$, $1 \times 1.92 \text{ \AA-N}$, $1 \times 1.93 \text{ \AA-N}$, Cr(3) $2 \times 1.74 \text{ \AA-N}$, $1 \times 1.75 \text{ \AA-N}$, $1 \times 1.99 \text{ \AA-N}$, $1 \times 2.18 \text{ \AA-N}$, Cr(4) $2 \times 1.77 \text{ \AA-N}$, and $2 \times 1.78 \text{ \AA-N}$.

In the corners of the cell, there are four SiN_4 tetrahedra with interatomic distances of $1 \times 1.74 \text{ \AA-N}$, $2 \times 1.76 \text{ \AA-N}$, and $1 \times 1.83 \text{ \AA-N}$. Additionally, there is one SiN_5 polyhedron corner connected to one of the tetrahedra (atom–atom distances of $1 \times 1.72 \text{ \AA-N}$, $1 \times 1.77 \text{ \AA-N}$, $2 \times 1.78 \text{ \AA-N}$, and $1 \times 2.49 \text{ \AA-N}$), where chromium is completely located in the inner part of the unit cell, and the connection between polyhedra is formed via edges and corners (Figure 11a).

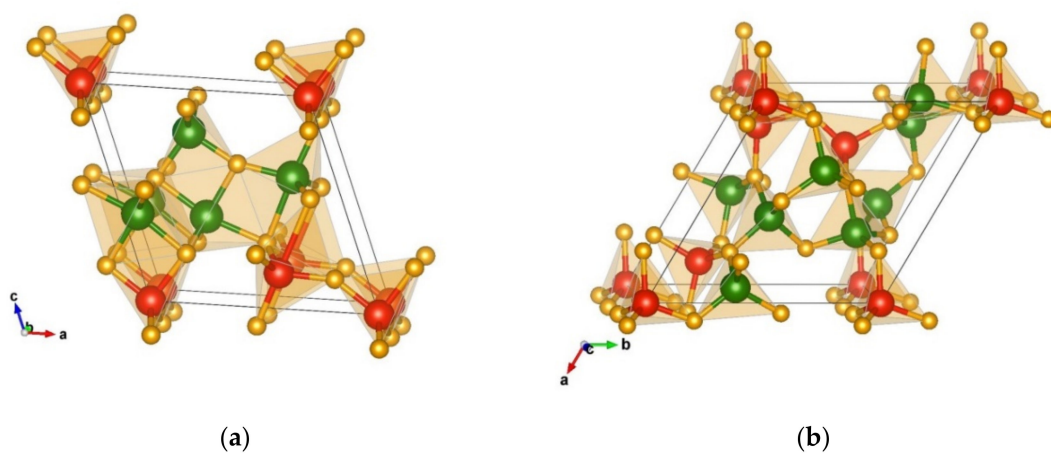


Figure 11. Visualization of the non-favorable PCAE structures: (a) Cr_2SiN_4 -PCAE-1-type in space group Pm (no. 6); (b) Cr_2SiN_4 -PCAE-2-type in space group $P1$ (no. 1). Green, red, and yellow spheres denote Cr, Si, and N atoms, respectively.

Structurally and energetically related is the Cr_2SiN_4 -PCAE-2-type of structure presented as a final non-favorable structure candidate generated using the PCAE method. In this case, the α -type structure of Si_3N_4 with trigonal $P31c$ (no. 159) space group [82,83] was used as starting point. However, after full structural optimization on the GGA-PBE level, the symmetry of the Cr_2SiN_4 -PCAE-2-type is completely reduced to space group $P1$ (no. 1) with unit cell parameters of $a = 7.87856$, $b = 7.96102$, $c = 5.78635$, $\alpha = 89.9706$, $\beta = 89.8616$, and $\gamma = 120.2646$ (Table 7).

Within this triclinic modification, both chromium and silicon are four-fold coordinated by nitrogen thus forming tetrahedra (Figure 11b). In this modification there are eight different CrN_4 tetrahedra, with the atom–atom distances Cr(1) $1 \times 1.77 \text{ \AA-N}$, $2 \times 1.80 \text{ \AA-N}$, $1 \times 1.86 \text{ \AA-N}$, Cr(2) $2 \times 1.78 \text{ \AA-N}$, $1 \times 1.79 \text{ \AA-N}$, $1 \times 1.81 \text{ \AA-N}$, Cr(3) $2 \times 1.79 \text{ \AA-N}$, $2 \times 1.80 \text{ \AA-N}$, Cr(4) $1 \times 1.77 \text{ \AA-N}$, $1 \times 1.78 \text{ \AA-N}$, $1 \times 1.80 \text{ \AA-N}$, $1 \times 1.81 \text{ \AA-N}$, Cr(5) $1 \times 1.77 \text{ \AA-N}$, $1 \times 1.79 \text{ \AA-N}$, $1 \times 1.81 \text{ \AA-N}$, $1 \times 1.87 \text{ \AA-N}$, Cr(6) $1 \times 1.78 \text{ \AA-N}$, $1 \times 1.80 \text{ \AA-N}$, $2 \times 1.82 \text{ \AA-N}$, Cr(7) $1 \times 1.78 \text{ \AA-N}$, $2 \times 1.79 \text{ \AA-N}$, $1 \times 1.81 \text{ \AA-N}$, Cr(8) $1 \times 1.78 \text{ \AA-N}$, $2 \times 1.79 \text{ \AA-N}$, and $1 \times 1.80 \text{ \AA-N}$.

Silicon is also four-fold coordinated by nitrogen resulting in two different SiN_4 tetrahedra with the interatomic distances Si1 $1 \times 1.73 \text{ \AA-N}$, $1 \times 1.74 \text{ \AA-N}$, $1 \times 1.75 \text{ \AA-N}$, $1 \times 1.76 \text{ \AA-N}$, Si2 $2 \times 1.74 \text{ \AA-N}$, and $2 \times 1.75 \text{ \AA-N}$. The SiN_4 tetrahedra are mostly positioned at the corners of the cell with three tetrahedra located inside along with CrN_4 tetrahedra located entirely inside the cell. Nevertheless, all tetrahedra within this phase are corner-connected (Figure 11b). A summary of the structural data of the presented PCAE structures is shown in Table 7; other structure candidates generated using the PCAE method were energetically much less favorable and, thus, have not been included.

Table 7. The modifications, space groups, unit cell parameters, and atomic positions for favorable Cr_2SiN_4 modifications found using the PCAE method and the GGA-PBE functional.

Modification and Space Group	Cell Parameters	Position of Atoms
γ - Cr_2SiN_4 -type <i>Cc</i> (no. 9)	$a = 5.62$ $b = 8.96$ $c = 5.36 \text{ \AA}$, $\beta = 117.93$	Cr 0.505134 0.354319 0.539894
		Cr 0.490988 0.640587 0.506788
		Si 0.000000 0.574728 0.000000
		N 0.820626 0.494637 0.668512
		N 0.339534 0.498028 0.687817
		N 0.683793 0.745757 0.858424
		N 0.673275 0.237591 0.860703
Cr_2SiN_4 -PCAE-1-type <i>Pm</i> (no. 6)	$a = 7.04$ $b = 3.04$ $c = 7.03$ $\beta = 110.72$	Cr 0.338406 0.500000 0.381358
		Cr 0.068281 0.000000 0.404484
		Cr 0.778353 0.500000 0.589017
		Cr 0.381419 0.500000 0.771064
		Si 0.000000 0.000000 0.000000
		Si 0.613136 0.000000 0.165992
		N 0.569205 0.500000 0.274738
		N 0.859037 0.000000 0.522005
		N 0.985060 0.500000 0.869495
		N 0.164949 0.500000 0.544984
		N 0.227376 0.000000 0.231306
		N 0.437810 0.000000 0.912940
N 0.551129 0.500000 0.636169		
N 0.853139 0.000000 0.153320		

Table 7. Cont.

Modification and Space Group	Cell Parameters	Position of Atoms
Cr ₂ SiN ₄ -PCAE-2-type <i>P1</i> (no. 1)	a = 7.88 b = 7.96 c = 5.79 α = 89.97 β = 89.86 γ = 120.26	Cr 0.179061 0.774468 0.214657
		Cr 0.576899 0.834251 0.216822
		Cr 0.514893 0.179271 0.216823
		Cr 0.596707 0.344636 0.708045
		Cr 0.010451 0.684706 0.713360
		Cr 0.678545 0.756495 0.700070
		Cr 0.343219 0.429431 0.991834
		Cr 0.923504 0.343769 0.996260
		Si 0.000000 0.000000 0.000000
		Si 0.263900 0.513623 0.496139
		Si 0.839296 0.185951 0.496185
		Si 0.163373 0.091041 0.497914
		N 0.743253 0.861393 0.985305
		N 0.495442 0.322138 0.989374
		N 0.052018 0.604045 0.985425
		N 0.711195 0.932465 0.477493
		N 0.419187 0.211059 0.484630
		N 0.145337 0.648381 0.483835
		N 0.406296 0.578413 0.243870
		N 0.773280 0.267856 0.250745
		N 0.088745 0.948405 0.247062
		N 0.418188 0.578819 0.734852
		N 0.770928 0.262416 0.742269
N 0.078587 0.945416 0.743265		
N 0.427572 0.932217 0.132893		
N 0.761872 0.590844 0.634583		
N 0.087863 0.251396 0.996965		
N 0.090039 0.265519 0.498530		

3.4. Energy Landscape of Cr₂SiN₄ on the Ab Initio Level

The global optimization, data mining, and PCAE based searches resulted in structure candidates that were, after detailed structural and crystallographic analysis, reduced to the eleven energetically most favorable Cr₂SiN₄ modifications. Table 8 presents the energetic ranking of these modifications, where the Al₂MgO₄-spinel-type appears lowest in calculated total energy with the value of $-5193.507 E_h$, thus, representing the global minimum among the candidates obtained in the various searches. If the calculations are performed using DFT-LDA (Table A2), the spinel structure remains the global minimum, and the energetic ranking of the other modifications is very similar, with few exceptions.

Figure 12 presents the energy versus volume ($E(V)$) curves on the ab initio level using the GGA-PBE functional for the energetically most favorable Cr₂SiN₄ modifications. We note that the global minimum in the Cr₂SiN₄ system is the Al₂MgO₄-spinel phase. This prominence of the Al₂MgO₄-type candidate on the energy landscape of Cr₂SiN₄ is not unreasonable, since several earlier calculations in the related (binary) Si₃N₄ system have also found a Al₂MgO₄-spinel-like phase [71,84,85].

At high-temperature conditions, one might expect structures, like the β -, ϵ -, λ -, and λ' -Cr₂SiN₄-type to possibly become competitive, as well as the TiMn₂O₄-type and Mg₂SiO₄-type modifications from the DM-based searches. Similarly, the most relevant modifications that might appear in the high-pressure region are the Na₂MnCl₄-type, and the α -, γ -, and δ -Cr₂SiN₄-types. Therefore, enthalpy vs. pressure, $H(p)$, curves were computed for these five modifications (Figure 13).

Table 8. The total energies and relative energy values compared to the global minimum (spinel structure taken as the zero of energy) of the energetically most favorable Cr_2SiN_4 modifications found using various search methods and later locally optimized on the ab initio level using the GGA-PBE functional. DM stands for data mining, GO stands for global optimization, and PCAE stands for Primitive Cell approach for Atom Exchange method.

Modification	Search Method	Total Energy (E_h)	Relative Energy (kcal/mol)
Al_2MgO_4 -spinel-type	DM	−5193.507	0.0
α - Cr_2SiN_4 -type	GO	−5193.474	20.708
β - Cr_2SiN_4 -type	GO	−5193.438	43.298
Na_2MnCl_4 -type	DM	−5193.436	44.553
γ - Cr_2SiN_4 -type	PCAE	−5193.435	45.181
δ - Cr_2SiN_4 -type	GO	−5193.419	55.221
TiMn_2O_4 -type	DM	−5193.414	58.358
ε - Cr_2SiN_4 -type	GO	−5193.413	58.986
λ - Cr_2SiN_4 -type	GO	−5193.407	62.750
λ' - Cr_2SiN_4 -type	GO	−5193.404	64.634
Mg_2SiO_4 -type	DM	−5193.403	65.261

A high-pressure phase transition was predicted between the spinel and the Na_2MnCl_4 -type at a pressure of ~ 33 GPa (Figure 13). In addition, there was a phase transition between the Na_2MnCl_4 -type and the metastable α - Cr_2SiN_4 -type modifications at ~ 15 GPa (Figure 13), i.e., the α -phase was more stable than the Na_2MnCl_4 -type modification below 15 GPa in the Cr_2SiN_4 system.

In summary, the energy landscape of Cr_2SiN_4 is highly complex with a wide range of structurally different modifications possible. On the ab initio level, the global minimum corresponds to the AlMg_2O_4 -type of structure. This modification is also known as a spinel structure, formulated as AB_2X_4 , with a fcc close-packed array of anions X, and A and B cations occupying some or all of the octahedral and tetrahedral sites in the lattice, respectively. The structural features found in this structure type are the most dominant ones in the low-energy region of the landscape of Cr_2SiN_4 at standard pressure, where most of the structures are found to exhibit an octahedral coordination of chromium by nitrogen and a tetrahedral one for silicon, respectively.

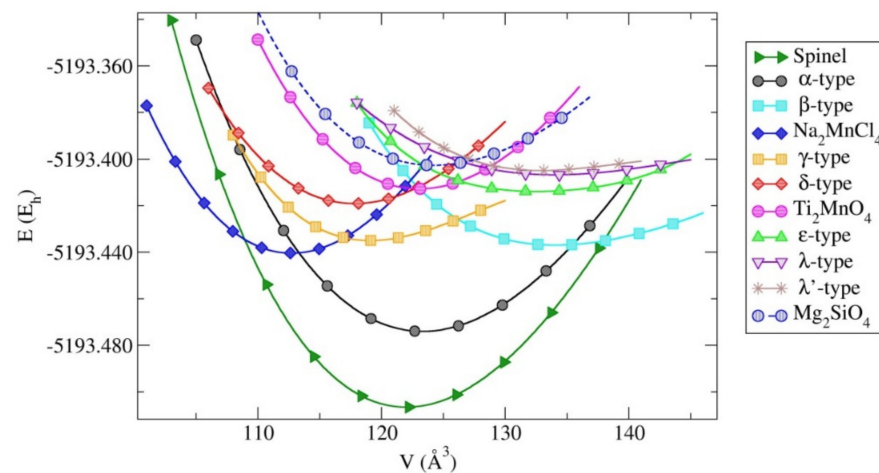


Figure 12. Energy vs. volume, $E(V)$, curves for the most favorable Cr_2SiN_4 modifications calculated using the GGA-PBE functional. Energies per formula unit are given in Hartree (E_h).

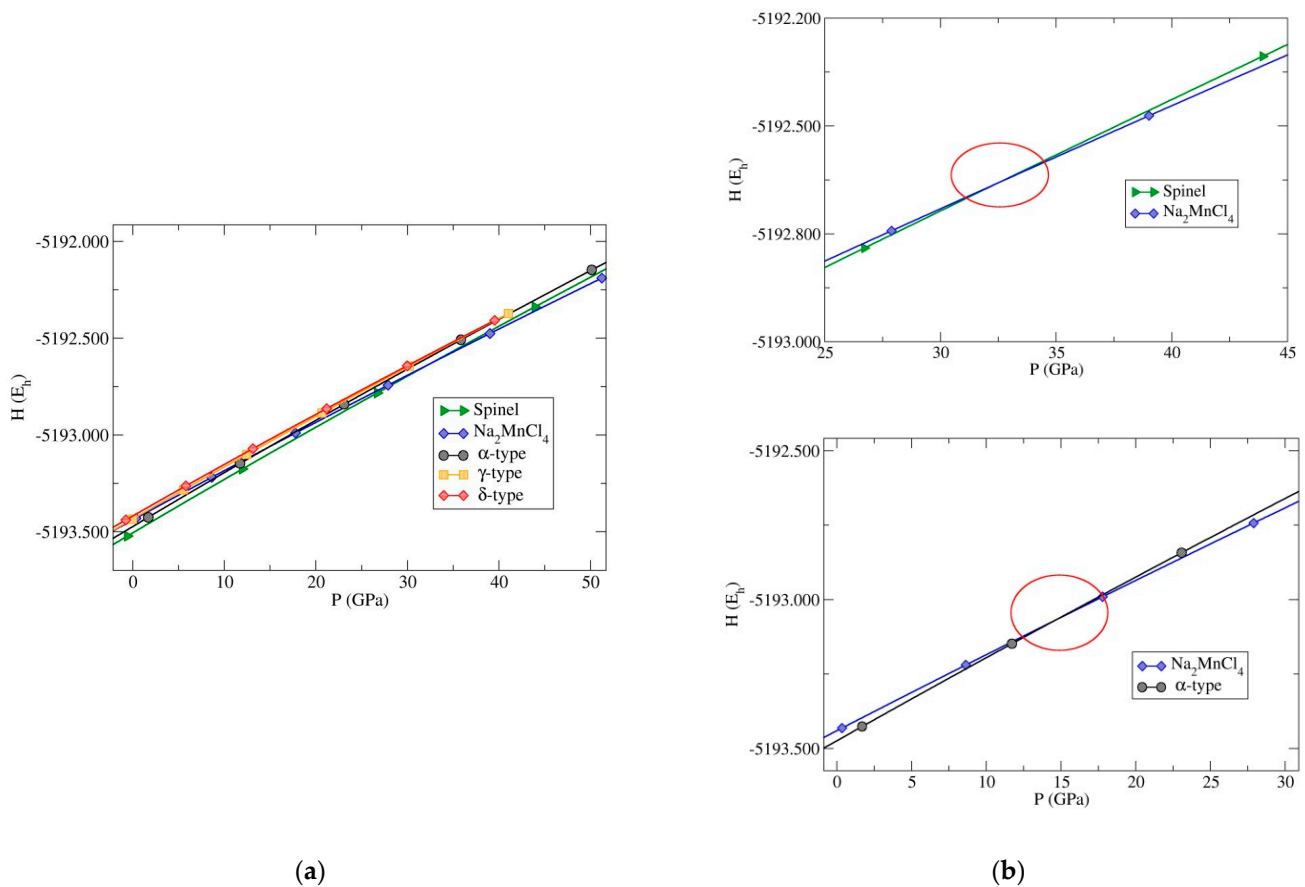


Figure 13. (a) Enthalpy vs. pressure, $H(p)$, curves computed for the five most relevant structures, including the high-pressure region. (b) Plots on the right side show $H(p)$ curves focused on two transitions. Top: $H(p)$ curves for the spinel and the Na_2MnCl_4 -type (transition pressure was found to be ~ 33 GPa); Bottom: $H(p)$ curves between the Na_2MnCl_4 -type and the α - Cr_2SiN_4 -type modifications (transition pressure would be ~ 15 GPa). The calculations were performed using the GGA-PBE functional and the energies per formula unit are given in Hartree (E_h).

However, some of the structure candidates observed exhibit six-fold coordination with an octahedral environment for both Cr and Si atoms (e.g., the γ - and the δ - Cr_2SiN_4 -type, the Na_2MnCl_4 -type, and the Mn_2SnS_4 -type), while there is only one stable modification (Cr_2SiN_4 -PCAE-2-type) exhibiting tetrahedral coordination by nitrogen for both cations. In addition, a few structures show unusual five-fold and seven-fold coordination, but these are energetically non-favorable.

The appearance of spinel as a global minimum in Cr_2SiN_4 and the observation of analogous coordination environments of Cr and Si in most of the structures found as low-energy minima on the landscape are strong indications that this compound should be synthetically accessible. Furthermore, a spinel-type modification of Cr_2SiN_4 could be of great importance, since ferrite spinels and related structures are of technological interest due to their magnetic ordering, which can be ferrimagnetic or antiferromagnetic depending on the structure and the nature of the metal ions.

Similarly, the results of recent investigations demonstrating that spinel coatings can be used to protect metals, such as chromium, from oxidation or corrosion, serve as another indication for the possible technological and industrial usefulness of the proposed Cr_2SiN_4 structure candidates [86–88]. Another interesting point is that the global minimum AlMg_2O_4 -spinel-type of the structure shows the highest cubic $Fd-3m$ symmetry, while most of the predicted structure candidates show much lower symmetry.

Here, we note that the spinel structure contains so many atoms that it was not feasible to be realized in the periodic simulation cell employed for the global optimizations; as a

consequence, the closely related α -Cr₂SiN₄-type structure was obtained instead. Quite generally, data-mining-based searches produced high-symmetry candidates (except for the HgC₂O₄-type, which is monoclinic), while global optimization and the PCAE method mostly produced structures with lower symmetry, with the orthorhombic space group *Pma2* (no. 28) of the α -Cr₂SiN₄-type as the highest symmetry space group.

We note that each of the methods used brought us a new perspective: data mining found the global minimum and suggested known structure types that can be stable in the Cr₂SiN₄ system, the global optimization resulted in a large number of new unknown but kinetically stable low-energy structures and provided a general overview over the broad structural variety present in the system at low energies, while the PCAE method generated the most diverse modifications, ranging from structures consisting of networks with only tetrahedral coordination polyhedra of the cations by nitrogen to modifications with only octahedral coordination environments.

4. Conclusions

A combination of global optimization, data mining, and the PCAE method was used to explore the energy landscape of Cr₂SiN₄ and to perform structure prediction in the Cr₂SiN₄ system. Global optimization was performed using simulated annealing and a fast computable robust empirical two-body potential. Data-mining-based searches reduced a large number of crystal structures from the ICSD database to four energetically favorable structures and five structure candidates that might be feasible modifications at extreme conditions for the not-yet-synthesized Cr₂SiN₄ compound.

Additionally, the Primitive Cell approach for Atom Exchange (PCAE) method was employed for generating alternative structure candidates in the Cr₂SiN₄ system with starting modifications taken from the related Si₃N₄ chemical system. Every structure candidate found in these searches was subjected to crystallographic analysis and all the promising ones to a local optimization on the ab initio level.

The local optimizations were performed on the DFT level employing the LDA-PZ and the GGA-PBE functional, for comparison, since there exists no experimental data that one could compare the results with. There was good agreement between the results from the two chosen functionals regarding the total energy ranking, space group symmetry, and other structural data of the various structure candidates after relaxation, which strongly supports the plausibility of the proposed candidates to correspond to actual (meta)stable modifications in the Cr₂SiN₄ system.

The explorations of the energy landscape of the Cr₂SiN₄ system resulted in numerous predicted new structures/modifications not yet observed in the experiment. Within each method used in this study, we grouped our results into energetically favorable and non-favorable Cr₂SiN₄ modifications, with the latter ones perhaps accessible for extreme thermodynamic conditions. Among the eleven energetically most favorable candidates, the global minimum was the AlMg₂O₄-spinel-type exhibiting the cubic *Fd-3m* symmetry.

At high pressures of ca. ~33 GPa, a phase transition between the spinel-type and the Na₂MnCl₄-type modifications should take place. Thus, we present a large number of feasible structures for modifications in the synthetically not-yet-explored Cr₂SiN₄ system, which might be suitable for many technological applications, such as high-speed cutting, wood machining applications, hydraulic piston pumps, valves, gears, shafts, and propellers, as corrosion-resistant coatings and low-cost water-based lubricating systems.

Author Contributions: Conceptualization, D.Z., B.M., J.C.S. and T.Š.; methodology, D.Z., M.P. and T.Š.; data curation, J.C.S., T.Š., D.Z. and M.P.; writing—original draft preparation, T.Š., D.Z. and M.P.; writing—review and editing, D.Z., B.M. and J.C.S. All authors have read and agreed to the published version of the manuscript.

Funding: This research was funded by the Ministry of Education, Science and Technological Development of Serbia (Project number: 1702001).

Data Availability Statement: Additional data may be requested from the first author.

Conflicts of Interest: The authors declare no conflict of interest.

Appendix A

Table A1. The modifications, space groups, unit cell parameters, and atomic positions for the most favorable Cr₂SiN₄ modifications after structural optimization on the DFT-LDA level.

Modifications and Space Groups	Cell Parameters	Position of Atoms
Al ₂ MgO ₄ -spinel-type_LDA <i>Fd-3m</i> No 227	a = 7.76	Cr 0.000000 0.000000 0.000000 Si 0.625000 0.625000 0.625000 N 0.752556 0.752556 0.752556
α-Cr ₂ SiN ₄ -type_LDA <i>Pma2</i> No 28	a = 5.45 b = 7.80 c = 2.76	Cr 0.750000 0.241721 0.552936 Cr 0.500000 0.000000 0.898141 Si 0.750000 0.614777 0.000000 N 0.750000 0.006165 0.421951 N 0.750000 0.489793 0.499478 N 0.501351 0.244258 0.983987
Na ₂ MnCl ₄ -type_LDA <i>Pbam</i> No 55	a = 4.67 b = 8.58 c = 2.69	Cr 0.432611 0.175929 0.500000 Si 0.000000 0.000000 0.000000 N 0.133271 0.203741 0.000000 N 0.257704 0.966687 0.500000
γ-Cr ₂ SiN ₄ -type_LDA <i>Cc</i> No 9	a = 5.56 b = 8.82 c = 5.25 β = 117.96	Cr 0.499339 0.356416 0.521849 Cr 0.490863 0.639616 0.502192 Si 0.000000 0.578114 0.000000 N 0.817340 0.495466 0.665199 N 0.336682 0.499101 0.681972 N 0.677149 0.750383 0.851076 N 0.670732 0.238989 0.855745
β-Cr ₂ SiN ₄ -type_LDA <i>P-1</i> No 2	a = 7.18 b = 7.69 c = 2.70 α = 94.01 β = 82.69 γ = 121.02	Cr 0.350127 0.864148 0.734578 Cr 0.863665 0.518329 0.302902 Si 0.625158 0.737213 0.910010 N 0.050410 0.680530 0.762885 N 0.352905 0.668370 0.167669 N 0.662487 0.971411 0.739846 N 0.713401 0.667644 0.365727
δ-Cr ₂ SiN ₄ -type_LDA <i>P21/m</i> No 11	a = 6.14 b = 3.76 c = 5.41 β = 115.88	Cr 0.091491 0.750000 0.659687 Cr 0.148173 0.750000 0.246670 Si 0.610570 0.750000 0.913336 N 0.638880 0.250000 0.419381 N 0.142755 0.250000 0.721438 N 0.367862 0.750000 0.044580 N 0.131910 0.250000 0.172992
TiMn ₂ O ₄ -type_LDA <i>P4322</i> No 95	a = 5.56 c = 7.61	Cr 0.500000 0.290089 0.000000 Cr 0.233800 0.233800 0.625000 Si 0.000000 0.260505 0.000000 N 0.238872 0.500821 0.998335 N 0.247363 0.028667 0.009638
Mg ₂ SiO ₄ -type_LDA <i>Pnma</i> No 62	a = 9.23 b = 5.35 c = 4.77	Cr 0.500000 0.500000 0.500000 Cr 0.752388 0.750000 0.005094 Si 0.911386 0.750000 0.581141 N 0.915976 0.750000 0.228570 N 0.580994 0.750000 0.754642 N 0.831042 0.496221 0.748887

Table A1. Cont.

Modifications and Space Groups	Cell Parameters	Position of Atoms
ϵ -Cr ₂ SiN ₄ -type_LDA <i>P21/m</i> No 11	a = 5.07 b = 2.86 c = 8.45 $\beta = 90.40$	Cr 0.780604 0.250000 0.510721
		Cr 0.923710 0.750000 0.845133
		Si 0.427115 0.250000 0.804711
		N 0.570806 0.750000 0.868258
		N 0.885468 0.750000 0.109395
		N 0.589494 0.750000 0.396942
		N 0.052827 0.250000 0.362060
λ -Cr ₂ SiN ₄ -type_LDA <i>Pm</i> No 6	a = 4.96 b = 2.84 c = 8.88 $\beta = 98.40$	Cr 0.914225 0.500000 0.418382
		Cr 0.707639 0.500000 0.700020
		Cr 0.303954 0.000000 0.721261
		Cr 0.508118 0.500000 0.052804
		Si 0.000000 0.000000 0.000000
		Si 0.419874 0.000000 0.378878
		N 0.545716 0.000000 0.572397
		N 0.460020 0.500000 0.846268
		N 0.704067 0.000000 0.081337
		N 0.551407 0.500000 0.308625
		N 0.057263 0.500000 0.603299
		N 0.068995 0.000000 0.346274
		N 0.943534 0.000000 0.807418
N 0.155450 0.500000 0.072091		
λ' -Cr ₂ SiN ₄ -type_LDA <i>Pm</i> No 6	a = 4.99 b = 2.82 c = 8.84 $\beta = 90.95$	Cr 0.175453 0.500000 0.329781
		Cr 0.898546 0.500000 0.677506
		Cr 0.311343 0.000000 0.668615
		Cr 0.483688 0.500000 0.973214
		Si 0.000000 0.000000 0.000000
		Si 0.681904 0.000000 0.380834
		N 0.683473 0.000000 0.573821
		N 0.506564 0.500000 0.783113
		N 0.663254 0.000000 0.037342
		N 0.818343 0.500000 0.305474
		N 0.181392 0.500000 0.535694
		N 0.363881 0.000000 0.300294
		N 0.023309 0.000000 0.806317
N 0.153474 0.500000 0.070996		

Table A2. The total energy and relative energy values compared to the global minimum (spinel structure taken as the zero of energy) of the energetically most favorable Cr₂SiN₄ modifications found using various search methods and later locally optimized on the ab initio level using the LDA-PZ functional. DM stands for data mining, GO stands for global optimization, and PCAE stands for primitive cell approach for atom exchange methods.

Modification and Space Group	Search Method	Total Energy (Eh)	Relative Energy (kcal/mol)
Al ₂ MgO ₄ -spinel-type_LDA	DM	-5180.729	0.0
α -Cr ₂ SiN ₄ -type_LDA	GO	-5180.694	21.963
Na ₂ MnCl ₄ -type_LDA	DM	-5180.672	35.768
γ -Cr ₂ SiN ₄ -type_LDA	PCAE	-5180.667	38.906
β -Cr ₂ SiN ₄ -type_LDA	GO	-5180.653	47.691
δ -Cr ₂ SiN ₄ -type_LDA	GO	-5180.653	47.691
TiMn ₂ O ₄ -type_LDA	DM	-5180.621	67.771
Mg ₂ SiO ₄ -type_LDA	DM	-5180.620	68.399
ϵ -Cr ₂ SiN ₄ -type_LDA	GO	-5180.615	71.536
λ -Cr ₂ SiN ₄ -type_LDA	GO	-5180.606	77.184
λ' -Cr ₂ SiN ₄ -type_LDA	GO	-5180.604	78.439

References

1. Benlatreche, Y.; Nouveau, C.; Aknouche, H.; Imhoff, L.; Martin, N.; Gavaille, J.; Rousselot, C.; Rauch, J.-Y.; Pilloud, D. Physical and Mechanical Properties of CrAlN and CrSiN Ternary Systems for Wood Machining Applications. *Plasma Process. Polym.* **2009**, *6*, S113–S117. [\[CrossRef\]](#)
2. Wang, H.; Ye, Y.; Wang, Y. Structure, corrosion, and tribological properties of CrSiN coatings with various Si contents in 3.5% NaCl solution. *Surf. Interface Anal.* **2018**, *50*, 471–479. [\[CrossRef\]](#)
3. Yang, D.; Chen, H.; Ye, Y.; Wang, C.; Zhao, H.; Gong, D. Doping silicon to enhance the anti-corrosion and anti-wear abilities of chromium nitride coating in seawater. *Surf. Topogr. Metrol. Prop.* **2018**, *6*, 044001. [\[CrossRef\]](#)
4. Iwasaki, Y.; Mizuno, Y.; Nakayama, T.; Suzuki, T. Preparation of Cr–Si–N–O thin films epitaxially grown on MgO substrates by pulsed laser deposition. *Vacuum* **2020**, *179*, 109498. [\[CrossRef\]](#)
5. Merces, D.; Bonasso, N.; Naamane, S.; Bordes, J.-M.; Coddet, C. Mechanical and tribological properties of Cr–N and Cr–Si–N coatings reactively sputter deposited. *Surf. Coat. Technol.* **2005**, *200*, 403–407. [\[CrossRef\]](#)
6. Kim, J.W.; Kim, K.H.; Lee, D.; Moore, J. Study on high-temperature oxidation behaviors of Cr–Si–N films. *Surf. Coat. Technol.* **2006**, *200*, 6702–6705. [\[CrossRef\]](#)
7. Lee, J.-W.; Kuo, Y.-C.; Wang, C.-J.; Chang, L.-C.; Liu, K.-T. Effects of substrate bias frequencies on the characteristics of chromium nitride coatings deposited by pulsed DC reactive magnetron sputtering. *Surf. Coat. Technol.* **2008**, *203*, 721–725. [\[CrossRef\]](#)
8. Dinu, M.; Mouele, E.S.M.; Parau, A.C.; Vladescu, A.; Petrik, L.F.; Braic, M. Enhancement of the Corrosion Resistance of 304 Stainless Steel by Cr–N and Cr(N,O) Coatings. *Coatings* **2018**, *8*, 132. [\[CrossRef\]](#)
9. Meng, C.; Yang, L.; Wu, Y.; Tan, J.; Dang, W.; He, X.; Ma, X. Study of the oxidation behavior of CrN coating on Zr alloy in air. *J. Nucl. Mater.* **2019**, *515*, 354–369. [\[CrossRef\]](#)
10. Lin, J.; Zhang, N.; Sproul, W.D.; Moore, J.J. A comparison of the oxidation behavior of CrN films deposited using continuous dc, pulsed dc and modulated pulsed power magnetron sputtering. *Surf. Coat. Technol.* **2012**, *206*, 3283–3290. [\[CrossRef\]](#)
11. Shan, L.; Wang, Y.; Li, J.; Jiang, X.; Chen, J. Improving tribological performance of CrN coatings in seawater by structure design. *Tribol. Int.* **2015**, *82*, 78–88. [\[CrossRef\]](#)
12. Shah, H.N.; Jayaganthan, R.; Kaur, D. Influence of reactive gas and temperature on structural properties of magnetron sputtered CrSiN coatings. *Appl. Surf. Sci.* **2011**, *257*, 5535–5543. [\[CrossRef\]](#)
13. Wo, P.; Munroe, P.; Li, Z.; Jiang, Z.-T.; Xie, Z.; Zhou, Z.; Li, K.Y. Factors governing the mechanical behaviour of CrSiN coatings: Combined nanoindentation testing and transmission electron microscopy. *Mater. Sci. Eng. A* **2012**, *534*, 297–308. [\[CrossRef\]](#)
14. Bobzin, K.; Bagcivan, N.; Immich, P.; Bolz, S.; Cremer, R.; Leyendecker, T. Mechanical properties and oxidation behaviour of (Al,Cr)N and (Al,Cr,Si)N coatings for cutting tools deposited by HPPMS. *Thin Solid Films* **2008**, *517*, 1251–1256. [\[CrossRef\]](#)
15. Vepřek, S. New development in superhard coatings: The superhard nanocrystalline-amorphous composites. *Thin Solid Films* **1998**, *317*, 449–454. [\[CrossRef\]](#)
16. Morgiel, J.; Grzonka, J.; Mania, R.; Zimowski, S.; Lábár, J.L.; Fogarassy, Z. Relation between microstructure and hardness of nano-composite CrN/Si₃N₄ coatings obtained using CrSi single target magnetron system. *Vacuum* **2013**, *90*, 170–175. [\[CrossRef\]](#)
17. Martinez, E.; Sanjinés, R.; Karimi, A.; Esteve, J.; Lévy, F. Mechanical properties of nanocomposite and multilayered Cr–Si–N sputtered thin films. *Surf. Coat. Technol.* **2004**, *180–181*, 570–574. [\[CrossRef\]](#)
18. Park, J.H.; Chung, W.S.; Cho, Y.-R.; Kim, K.H. Synthesis and mechanical properties of Cr–Si–N coatings deposited by a hybrid system of arc ion plating and sputtering techniques. *Surf. Coat. Technol.* **2004**, *188–189*, 425–430. [\[CrossRef\]](#)
19. Lin, H.-H.; Chou, C.-C.; Lee, J.-W. Tribological properties of Cr–Si–N nanocomposite film adherent silicon under various environments. *Thin Solid Films* **2010**, *518*, 7509–7514. [\[CrossRef\]](#)
20. Azzi, M.; Benkahoul, M.; Szpunar, J.; Klemberg-Sapieha, J.; Martinu, L. Tribological properties of CrSiN-coated 301 stainless steel under wet and dry conditions. *Wear* **2009**, *267*, 882–889. [\[CrossRef\]](#)
21. Lee, J.-W.; Chang, Y.-C. A study on the microstructures and mechanical properties of pulsed DC reactive magnetron sputtered Cr–Si–N nanocomposite coatings. *Surf. Coat. Technol.* **2007**, *202*, 831–836. [\[CrossRef\]](#)
22. Lee, H.; Jung, W.; Han, J.; Seo, S.; Kim, J.; Bae, Y. The synthesis of CrSiN film deposited using magnetron sputtering system. *Surf. Coat. Technol.* **2005**, *200*, 1026–1030. [\[CrossRef\]](#)
23. Zhang, G.; Wang, L.; Wang, S.; Yan, P.; Xue, Q. Structure and mechanical properties of reactive sputtering CrSiN films. *Appl. Surf. Sci.* **2009**, *255*, 4425–4429. [\[CrossRef\]](#)
24. Geng, Z.; Wang, H.; Wang, C.; Wang, L.; Zhang, G. Effect of Si content on the tribological properties of CrSiN films in air and water environments. *Tribol. Int.* **2014**, *79*, 140–150. [\[CrossRef\]](#)
25. Shao, T.; Ge, F.; Pei, C.; Huang, F.; Sun, D.; Zhang, S. Effects of Si content on Tribo-corrosion behavior of Cr_{1-x}Si_xN coatings prepared via magnetron sputtering. *Surf. Coat. Technol.* **2018**, *356*, 11–18. [\[CrossRef\]](#)
26. Shan, L.; Zhang, Y.-R.; Wang, Y.-X.; Li, J.-L.; Jiang, X.; Chen, J.-M. Corrosion and wear behaviors of PVD CrN and CrSiN coatings in seawater. *Trans. Nonferr. Met. Soc. China* **2016**, *26*, 175–184. [\[CrossRef\]](#)
27. Park, I.-W.; Kang, D.S.; Moore, J.J.; Kwon, S.C.; Rha, J.J.; Kim, K.H. Microstructures, mechanical properties, and tribological behaviors of Cr–Al–N, Cr–Si–N, and Cr–Al–Si–N coatings by a hybrid coating system. *Surf. Coat. Technol.* **2007**, *201*, 5223–5227. [\[CrossRef\]](#)
28. Lu, S.; Wang, Y.; Gaoand, P.; Meng, D. Effect of Si Content on Structure and Friction and Wear Properties of CrSiN Coatings. *IOP Conf. Ser. Earth Environ. Sci.* **2020**, *440*, 022028. [\[CrossRef\]](#)

29. Wang, Q.; Lin, Y.; Zhou, F.; Kong, J. The influence of Ni concentration on the structure, mechanical and tribological properties of Ni–CrSiN coatings in seawater. *J. Alloy. Compd.* **2020**, *819*, 152998. [[CrossRef](#)]
30. Kim, G.; Kim, B.; Lee, S. High-speed wear behaviors of CrSiN coatings for the industrial applications of water hydraulics. *Surf. Coat. Technol.* **2005**, *200*, 1814–1818. [[CrossRef](#)]
31. Chang, W.J.; Zhang, H.; Chen, Y.Y.; Li, J.; Zhang, X.; Jiang, P.Z.; Fan, X.W.; Duo, S.W. Tribological Performances of CrSiN Coatings Deposited by High Power Pulse Magnetron Sputtering. *Solid State Phenom.* **2018**, *281*, 540–545. [[CrossRef](#)]
32. Lou, B.-S.; Chang, Y.-C.; Lee, J.-W. High Temperature Oxidation Behaviors of CrN_x and Cr-Si-N Thin Films at 1000 °C. *Coatings* **2019**, *9*, 540. [[CrossRef](#)]
33. Mikula, M.; Grančič, B.; Drienovsky, M.; Satrapinskyy, L.; Roch, T.; Hájovská, Z.; Gregor, M.; Plecenik, T.; Čička, R.; Kúš, P. Thermal stability and high-temperature oxidation behavior of Si–Cr–N coatings with high content of silicon. *Surf. Coat. Technol.* **2013**, *232*, 349–356. [[CrossRef](#)]
34. Suzuki, K.; Suzuki, T.; Endo, T.; Nakayama, T.; Suematsu, H.; Niihara, K. Epitaxial growth of chromium nitride thin films with addition of silicon. *Phys. Status Solidi* **2015**, *12*, 545–548. [[CrossRef](#)]
35. Xu, X.M.; Zhang, H.; Luo, F.F.; Zhou, Z.H.; Duo, S.W. The Properties of CrSiN Coatings of Different Si Content. *Appl. Mech. Mater.* **2014**, *687–691*, 4323–4326. [[CrossRef](#)]
36. Wang, Q.M.; Kim, K.H. Microstructural control of Cr–Si–N films by a hybrid arc ion plating and magnetron sputtering process. *Acta Mater.* **2009**, *57*, 4974–4987. [[CrossRef](#)]
37. Martínez, E.; Sanjinés, R.; Banakh, O.; Lévy, F. Electrical, optical and mechanical properties of sputtered CrN_y and Cr_{1–x}Si_xN_{1.02} thin films. *Thin Solid Films* **2004**, *447–448*, 332–336. [[CrossRef](#)]
38. Ma, B.; Luo, B.; Wang, Z.; Meng, C.; He, X. Friction and Wear Properties of CrAl-Based Coatings for Nuclear Fuel Cladding. *Front. Energy Res.* **2021**, *9*, 24. [[CrossRef](#)]
39. Zagorac, J.; Schön, J.C.; Matović, B.; Škundrić, T. Predicting Feasible Modifications of Ce₂ON₂ Using a Combination of Global Optimization and Data Mining. *J. Phase Equilibria Diffus.* **2020**, *41*, 538–549. [[CrossRef](#)]
40. Zagorac, D.; Zagorac, J.; Schön, J.C.; Stojanović, N.; Matović, B. ZnO/ZnS (hetero)structures: Ab initio investigations of polytypic behavior of mixed ZnO and ZnS compounds. *Acta Crystallogr. Sect. B Struct. Sci. Cryst. Eng. Mater.* **2018**, *74*, 628–642. [[CrossRef](#)]
41. Kirkpatrick, S.; Gelatt, C.D.; Vecchi, M.P. Optimization by Simulated Annealing. *Science* **1983**, *220*, 671–680. [[CrossRef](#)] [[PubMed](#)]
42. Schön, J.C. Nanomaterials—What energy landscapes can tell us. *Process. Appl. Ceram.* **2015**, *9*, 157–168. [[CrossRef](#)]
43. Schön, J.C.; Jansen, M. Determination of candidate structures for simple ionic compounds through cell optimisation. *Comput. Mater. Sci.* **1995**, *4*, 43–58. [[CrossRef](#)]
44. Bergerhoff, G.; Brown, I.D. *Crystallographic Databases*; Allen, F.H., Bergerhoff, G., Sievers, R., Eds.; International Union of Crystallography: Chester, UK, 1987.
45. Zagorac, D.; Müller, H.; Ruehl, S.; Rehme, S. Recent developments in the Inorganic Crystal Structure Database: Theoretical crystal structure data and related features. *J. Appl. Crystallogr.* **2019**, *52*, 918–925. [[CrossRef](#)]
46. Zagorac, J.; Rosic, M.; Schön, J.C.; Matovic, B. Structure prediction of aluminum nitride combining data mining and quantum mechanics. *CrystEngComm* **2017**, *19*, 5259–5268. [[CrossRef](#)]
47. Cvijović-Alagić, I.; Rakin, M.; Laketić, S.; Zagorac, D. Microstructural study of Ti₄₅Nb alloy before and after HPT processing using experimental and *ab initio* data mining approach. *Mater. Charact.* **2020**, *169*, 110635. [[CrossRef](#)]
48. Zagorac, J.; Jovanovic, D.; Volkov-Husovic, T.; Matovic, B.; Zagorac, D. Structure prediction, high pressure effect and properties investigation of superhard B₆O. *Model. Simul. Mater. Sci. Eng.* **2020**, *28*. [[CrossRef](#)]
49. Dovesi, R.; Erba, A.; Orlando, R.; Zicovich-Wilson, C.M.; Civalleri, B.; Maschio, L.; Rérat, M.; Casassa, S.; Baima, J.; Salustro, S.; et al. Quantum-mechanical condensed matter simulations with CRYSTAL. *Wiley Interdiscip. Rev. Comput. Mol. Sci.* **2018**, *8*, e1360. [[CrossRef](#)]
50. Dovesi, R.; Pascale, F.; Civalleri, B.; Doll, K.; Harrison, N.M.; Bush, I.; D’Arco, P.; Noël, Y.; Rérat, M.; Carbonnière, P.; et al. The CRYSTAL code, 1976–2020 and beyond, a long story. *J. Chem. Phys.* **2020**, *152*, 204111. [[CrossRef](#)] [[PubMed](#)]
51. Doll, K.; Saunders, V.R.; Harrison, N.M. Analytical Hartree–Fock gradients for periodic systems. *Int. J. Quantum Chem.* **2001**, *82*, 1–13. [[CrossRef](#)]
52. Doll, K.; Dovesi, R.; Orlando, R. Analytical Hartree–Fock gradients with respect to the cell parameter for systems periodic in three dimensions. *Theor. Chem. Acc.* **2004**, *112*, 394–402. [[CrossRef](#)]
53. Perdew, J.P.; Zunger, A. Self-interaction correction to density-functional approximations for many-electron systems. *Phys. Rev. B* **1981**, *23*, 5048–5079. [[CrossRef](#)]
54. Perdew, J.P.; Burke, K.; Ernzerhof, M. Generalized gradient approximation made simple. *Phys. Rev. Lett.* **1996**, *77*, 3865–3868. [[CrossRef](#)]
55. Schön, J.C.; Čančarević, Ž.; Jansen, M. Structure prediction of high-pressure phases for alkali metal sulfides. *J. Chem. Phys.* **2004**, *121*, 2289–2304. [[CrossRef](#)] [[PubMed](#)]
56. Zagorac, D.; Doll, K.; Schön, J.C.; Jansen, M. Ab initio structure prediction for lead sulfide at standard and elevated pressures. *Phys. Rev. B* **2011**, *84*, 045206. [[CrossRef](#)]
57. Zagorac, J.; Schön, J.C.; Jansen, M. Prediction of structure candidates for zinc oxide as a function of pressure and investigation of their electronic properties. *Phys. Rev. B* **2014**, *89*, 075201. [[CrossRef](#)]

58. Catti, M.; Sandrone, G.; Valerio, G.; Dovesi, R. Electronic, magnetic and crystal structure of Cr_2O_3 by theoretical methods. *J. Phys. Chem. Solids* **1996**, *57*, 1735–1741. [[CrossRef](#)]
59. Ruiz, E.; Lluell, M.; Alemany, P. Calculation of exchange coupling constants in solid state transition metal compounds using localized atomic orbital basis sets. *J. Solid State Chem.* **2003**, *176*, 400–411. [[CrossRef](#)]
60. Pascale, F.; Zicovich-Wilson, C.; Orlando, R.; Roetti, C.; Ugliengo, P.; Dovesi, R. Vibration Frequencies of $\text{Mg}_3\text{Al}_2\text{Si}_3\text{O}_{12}$ Pyrope. An ab Initio Study with the CRYSTAL Code. *J. Phys. Chem. B* **2005**, *109*, 6146–6152. [[CrossRef](#)] [[PubMed](#)]
61. Noel, Y.; Catti, M.; D'Arco, P.; Dovesi, R. The vibrational frequencies of forsterite Mg_2SiO_4 : An all-electron ab initio study with the CRYSTAL code. *Phys. Chem. Miner.* **2006**, *33*, 383–393. [[CrossRef](#)]
62. Dovesi, R.; Causa', M.; Orlando, R.; Roetti, C.; Saunders, V.R. Ab initio approach to molecular crystals: A periodic Hartree–Fock study of crystalline urea. *J. Chem. Phys.* **1990**, *92*, 7402–7411. [[CrossRef](#)]
63. Zagorac, D.; Djukic, M.; Jordanov, D.; Matović, B. Theoretical study of AlN mechanical behaviour under high pressure regime. *Theor. Appl. Fract. Mech.* **2019**, *103*, 102289. [[CrossRef](#)]
64. Hundt, R.; Schön, J.C.; Hannemann, A.; Jansen, M. Determination of symmetries and idealized cell parameters for simulated structures. *J. Appl. Crystallogr.* **1999**, *32*, 413–416. [[CrossRef](#)]
65. Hannemann, A.; Hundt, R.; Schön, J.C.; Jansen, M. A New Algorithm for Space-Group Determination. *J. Appl. Crystallogr.* **1998**, *31*, 922–928. [[CrossRef](#)]
66. Hundt, R.; Schön, J.C.; Jansen, M. CMPZ— an algorithm for the efficient comparison of periodic structures. *J. Appl. Crystallogr.* **2006**, *39*, 6–16. [[CrossRef](#)]
67. Hundt, R. *KPLOT: A Program for Plotting and Analysing Crystal Structures*; Technicum Scientific Publishing: Stuttgart, Germany, 2016.
68. Momma, K.; Izumi, F. VESTA 3 for three-dimensional visualization of crystal, volumetric and morphology data. *J. Appl. Crystallogr.* **2011**, *44*, 1272–1276. [[CrossRef](#)]
69. Cui, L.; Hu, M.; Wang, Q.; Xu, B.; Yu, D.; Liu, Z.; He, J. Prediction of novel hard phases of Si_3N_4 : First-principles calculations. *J. Solid State Chem.* **2015**, *228*, 20–26. [[CrossRef](#)]
70. Yamanaka, T.; Takéuchi, Y. Order-disorder transition in MgAl_2O_4 spinel at high temperatures up to 1700 °C. *Z. Krist.* **1983**, *165*, 65–78. [[CrossRef](#)]
71. Kroll, P. Pathways to metastable nitride structures. *J. Solid State Chem.* **2003**, *176*, 530–537. [[CrossRef](#)]
72. Goodyear, J.; Ali, S.A.D.; Steigmann, G.A. The crystal structure of Na_2MnCl_4 . *Acta Crystallogr. Sect. B Struct. Crystallogr. Cryst. Chem.* **1971**, *27*, 1672–1674. [[CrossRef](#)]
73. Bertaut, E.; Vincent, H. Etude par diffraction neutronique de la forme ordonnée de l'orthotitanate de manganese-structure cristalline et structure magnétique. *Solid State Commun.* **1968**, *6*, 269–275. [[CrossRef](#)]
74. Smyth, J.; Hazen, R. The crystal structures of forsterite and hortonolite at several temperatures up to 900 °C. *Am. Mineral.* **1973**, *58*, 588–593.
75. Friedt, O.; Braden, M.; André, G.; Adelman, P.; Nakatsuji, S.; Maeno, Y. Structural and magnetic aspects of the metal-insulator transition in $\text{Ca}_{2-x}\text{Sr}_x\text{RuO}_4$. *Phys. Rev. B* **2001**, *63*, 174432. [[CrossRef](#)]
76. Christensen, A.N.; Norby, P.; Hanson, J.C. A crystal structure determination of HgC_2O_4 from synchrotron X-ray and neutron powder diffraction data. *Z. Krist. Cryst. Mater.* **1994**, *209*, 874–877. [[CrossRef](#)]
77. Matar, S.F.; Etourneau, J. $(\text{CaO})_n\text{IrO}_2$ ($n = 1, 2, 4$) family: Chemical scissors effects of CaO on structural characteristics correlated to physical properties. Ab initio study. *J. Solid State Chem.* **2017**, *255*, 82–88. [[CrossRef](#)]
78. Shashkin, D.P.; Simonov, M.A.; Belov, N.V. Crystalline structure of calciborite— $\text{CaB}_2\text{O}_4 = \text{Ca}_2[\text{BO}_3\text{BO}]_2$. *Dokl. Akad. Nauk SSSR* **1970**, *195*, 345–348.
79. Partik, M.; Stingl, T.; Lutz, H.D.; Sabrowsky, H.; Vogt, P. Strukturverfeinerung und magnetische Messungen an Mn_2SnS_4 . *Z. Anorg. Allg. Chem.* **1995**, *621*, 1600–1604. [[CrossRef](#)]
80. Hahn, H.; Klingler, W. Zur Struktur des $\beta\text{Cu}_2\text{Hg}_4$ und des $\beta\text{-Ag}_2\text{Hg}_4$. *Z. Anorg. Allg. Chem.* **1955**, *279*, 271–280. [[CrossRef](#)]
81. Schneider, J.; Johnson, F.N.; Laschke, K. Structure refinements of $\beta\text{-Si}_3\text{N}_4$ at temperatures up to 1360 °C by X-ray powder investigation. *Z. Krist. Cryst. Mater.* **1994**, *209*, 328–333. [[CrossRef](#)]
82. Yang, P.; Fun, H.K.; Rahman, I.A.; Saleh, M. Two phase refinements of the structures of $\alpha\text{-Si}_3\text{N}_4$ and $\beta\text{-Si}_3\text{N}_4$ made from rice husk by Rietveld analysis. *Ceram. Int.* **1995**, *21*, 137–142. [[CrossRef](#)]
83. Toraya, H. Crystal structure refinement of $\alpha\text{-Si}_3\text{N}_4$ using synchrotron radiation powder diffraction data: Unbiased refinement strategy. *J. Appl. Crystallogr.* **2000**, *33*, 95–102. [[CrossRef](#)]
84. Kroll, P.; Milko, M. Theoretical Investigation of the Solid State Reaction of Silicon Nitride and Silicon Dioxide forming Silicon Oxynitride ($\text{Si}_2\text{N}_2\text{O}$) under Pressure. *Z. Anorg. Allg. Chem.* **2003**, *629*, 1737–1750. [[CrossRef](#)]
85. Wang, H.; Chen, Y.; Kaneta, Y.; Iwata, S. First-principles investigation of the structural, electronic and optical properties of olivine- Si_3N_4 and olivine- Ge_3N_4 . *J. Phys. Condens. Matter* **2006**, *18*, 10663–10676. [[CrossRef](#)]
86. Wang, R.; Sun, Z.; Pal, U.B.; Gopalan, S.; Basu, S.N. Mitigation of chromium poisoning of cathodes in solid oxide fuel cells employing $\text{CuMn}_{1.8}\text{O}_4$ spinel coating on metallic interconnect. *J. Power Sources* **2018**, *376*, 100–110. [[CrossRef](#)]
87. Hassan, M.A.; Mamat, O.B. Mitigation of Chromium Poisoning of Ferritic Interconnect from Annealed Spinel of CuFe_2O_4 . *Processes* **2020**, *8*, 1113. [[CrossRef](#)]
88. Rose, L. *On the Degradation of Porous Stainless Steel in Low and Intermediate Temperature Solid Oxide Fuel Cell Support Materials*; University of British Columbia: Vancouver, BC, Canada, 2011.